Biotic transformation of methylmercury at the onset of the Arctic spring bloom

Stephen Kohler, Lars-Eric Heimbürger-Boavida, Philipp Assmy, Oliver Müller, Stefan Thiele, Maria Digernes, Kuria Ndungu, Murat Ardelan

To cite this version:

Stephen Kohler, Lars-Eric Heimbürger-Boavida, Philipp Assmy, Oliver Müller, Stefan Thiele, et al.. Biotic transformation of methylmercury at the onset of the Arctic spring bloom. Progress in Oceanography, inPress, 10.1016/j.pocean.2024.103224 . hal-04470915

HAL Id: hal-04470915
https://hal.science/hal-04470915

Biotic transformation of methylmercury at the onset of the Arctic spring bloom

Stephen G. Kohler[a], Lars-Eric Heimbürger-Boavida[b], Philipp Assmy[c], Oliver Müller[d], Stefan Thiele[d,e], Maria G. Digernes[a], Kuria Ndungu[f], Murat V. Ardelan[a]

[a]Department of Chemistry, Norwegian University of Science and Technology (NTNU), Høgskoleringen 5, NO-7491 Trondheim, Norway

[b]Aix-Marseille Université, CNRS/INSU, University de Toulon, IRD, Mediterranean Institute of Oceanography (MIO), Bât. Méditerranée, Campus de Luminy-Océanomed, 13009 Marseille, France

[c]Norwegian Polar Institute, Fram Centre, 9296, Tromsø, Norway

[d]Department of Biological Sciences, University of Bergen, Thormøhlensgate 53 A/B, 5006 Bergen, Norway

[e]Bjerknes Centre for Climate Research, Jahnebakken 5, 5007 Bergen, Norway

[f]Norwegian Institute for Water Research (NIVA), Økernveien 94, NO-0579 Oslo, Norway

Graphical Abstract

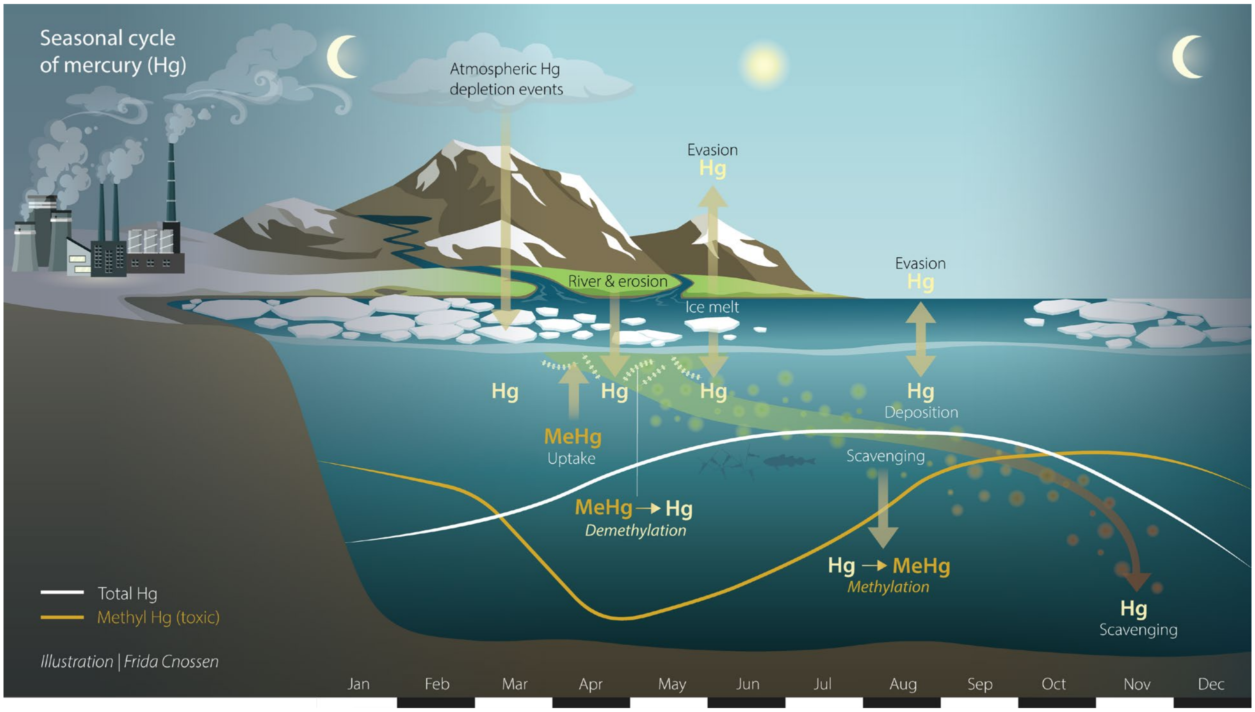

Keywords

Barents Sea, mercury, seasonality, Arctic Ocean, spring bloom

Abstract

Despite the lack of local anthropogenic mercury sources, methylated mercury (MeHg) concentrations in Arctic biota are higher than in biota from lower latitudes. The main entry route occurs during the bioconcentration of seawater monomethylmercury (MMHg) into phytoplankton. Despite the known seasonal changes in biological activity in the region, little is known about the seasonal cycling of total mercury (THg) and MeHg in the Arctic Ocean. Here, we report the concentrations of THg and MeHg in seawater sampled from the northwestern Barents Sea water column during late winter and spring. In the upper 500 m, the THg concentrations are significantly higher in spring (0.64 ± 0.09 pmol L^{-1}) compared to late winter (0.53 ± 0.07 pmol L^{-1}), driven by seasonal inputs to surface waters from atmospheric deposition and the dynamics of changing sea ice conditions. Contrastingly, the MeHg concentrations in spring were significantly lower (41 ± 39 fmol L^{-1}) compared to late winter (85 ± 42 fmol L^{-1}). We suggest that most MeHg is biotically demethylated by both phytoplankton and bacteria, with additional losses from photodemethylation and evasion. Our observations highlight the importance of demethylation during potential uptake of methylmercury coinciding with the Arctic spring bloom. Lastly, we use our new data together with previously published seasonal data in the region to construct a simplified seasonal mercury cycle in an Arctic marginal ice zone.

1 Introduction

The bioaccumulation of mercury (Hg) in the Arctic Ocean continues to remain an issue of concern for the marine ecosystem and indigenous peoples (Basu et al., 2022). Specifically, the bioconcentration of toxic monomethylmercury (MMHg) into phytoplankton and its subsequent bioaccumulation in the marine food web represents a risk to higher trophic level organisms (Dietz et al., 2022). The development and peak of primary productivity in the Arctic Ocean is restricted to the spring and summer (April to August), when light is available. In the spring, the phytoplankton bloom develops in the marginal ice zone (Strass and Nöthig, 1996; Reigstad et al., 2002). Several studies have highlighted phytoplankton blooms below fully consolidated sea ice as a result of the thinning and more dynamic icescape (Assmy et al., 2017, Ardyna et al., 2020).

Concurrently, the Arctic Ocean receives seasonal inputs of mostly inorganic Hg (iHg) via atmospheric deposition, riverine input, erosion, snow, glacial and sea ice melt (Dastoor et al., 2022). However, seasonal cycling of Hg in the water column in the Arctic region is still poorly understood (Kohler et al., 2022a). As the Arctic spring bloom provides a crucial transfer of energy and potentially Hg into higher trophic levels, more knowledge on the amount of Hg available for bioconcentration prior and during the Arctic spring bloom is needed. Seasonal inputs from thawing permafrost, glacial melt, and erosion are expected to deliver greater amounts of iHg to the biologically productive Arctic Ocean shelf seas in the future (Chételat et al., 2022) with most Hg expected to remain in the marine environment (Araujo et al., 2022). Hg can be scavenged to shelf sediments, advected with the halocline, cascaded into the deep basin (Dastoor et al., 2022) or potentially transported into the Central Arctic Ocean via the transpolar drift (Charette et al., 2020).

Several major Hg inputs to the Arctic region have strong seasonal patterns. Atmospheric mercury depletion events (AMDEs) (Schroeder et al., 1998) occur during polar sunrise in March and frequently occur throughout April, depositing iHg to snow, sea ice, and surface waters. Although a substantial fraction is photochemically reduced and reemitted back to the atmosphere as gaseous Hg^0 (Durnford and Dastoor 2011, Araujo et al., 2022), high concentrations of total Hg (THg) are seen in snow, sea ice and frost flowers (Dommergue et al., 2010, Chaulk et al., 2011). Sea ice, melting snow and glacial runoff can also provide additional Hg to the coastal and open ocean (Schartup et al., 2020, Kim et al., 2020a, Dastoor et al., 2022). Rivers also deliver large amounts of iHg from the snowpack, surface soils, thawing permafrost, and erosion to the Arctic shelf seas during a freshet in springtime (Sonke et al., 2018, Zolkos et al., 2020). While new evidence suggests seasonal cycling of iHg in the upper water column during autumn and early winter (Kohler et al., 2022a) with suspected surface losses to deeper waters and sediments with sinking particles, water column measurements of Hg species from late winter are scarce (Wang et al., 2012).

Arctic surface waters are elevated in THg during the summer (Heimbürger et al., 2015) from seasonal iHg inputs. Light reduces iHg to Hg^0 and photolytically degrades MeHg (Sellers et al., 1996). Gaseous Hg species can evade from the marginal ice zones (Yue et al., 2023) while ionic Hg species can be transported downward with sinking particles (Tesán Onrubia et al., 2020). Ionic

Hg is also often complexed to dissolved organic matter (DOM) and reduced sulfur compounds, which can affect Hg uptake and biogeochemical transformations between iHg and MeHg (Ravichandran 2004). During and after the phytoplankton bloom, bacterial remineralization of sinking particulate organic matter fuels in situ MeHg production, leading to elevated subsurface concentrations of MeHg in the marginal ice zones and the permanently ice-covered central Arctic Ocean (Heimbürger et al., 2015). However, sea ice hinders both photodemethylation (Point et al., 2009) and the evasion of gaseous species (Hg^0 and dimethylmercury (DMHg)) (DiMento et al., 2019). Gaseous Hg species potentially build up under and within the ice throughout winter (Andersson et al., 2008, Schartup et al., 2020). Hg that is removed from surface waters via sinking particles and delivered to bottom sediments may ultimately be methylated to MeHg (Kim et al., 2020b). Resuspension of fine-grained sediment and diffusion of porewater can deliver both iHg and MeHg back to subsurface Arctic waters (Kim et al., 2020b). While in situ incubations indicate Arctic waters can be in net states of methylation or demethylation (Lehnherr et al., 2011), the advection of outflowing Arctic waters indicate that the Arctic Ocean is a net producer of MeHg (Petrova et al., 2020, Jonsson et al., 2022a). Consequently, understanding the timing and magnitude of both Hg methylation and demethylation is important. Due to a limited number of observations, the fate of marine MeHg throughout the Arctic winter and during the transition to the spring bloom is unknown.

We hypothesized the potential seasonality of pelagic Hg species in the northern Barents Sea in the late winter to spring transition due to seasonal Hg inputs and biological development. We measured unfiltered THg (the sum of all mercury species) and unfiltered MeHg (the sum of MMHg and DMHg) in seawater, under ice water, and sea ice on two seasonal cruises in late winter (March) and spring (end of April-May). We report Hg concentrations from seven stations along a south-north transect and explore how hydrography, biological parameters, and seasonal processes affect our observations using literature and statistical relationships. We combine our Hg and environmental data with that of two other seasonal cruises in the region (Kohler et al., 2022a) to propose a simple seasonal model of the pelagic Hg cycle in surface waters of an Arctic marginal ice zone.

2 Materials & Methods

2.1 Oceanographic Conditions

The northern Barents Sea consists of water masses with both Atlantic Water (AW) and Polar Water (PW) origins (Sundfjord et al., 2020). AW, characteristic of warmer water with higher salinity, flows into the northern Barents Sea from the south through the Barents Sea Opening and through troughs in the north (Lundesgaard et al., 2022). This AW sinks below colder and fresher PW which arrives from the central Arctic Ocean and the Kara Sea in the east (Loeng 1991). The boundary between these two water masses is often referred to as the polar front, and generally delineates the extent of sea ice in the region. Surface PW with colder temperatures entering the northern Barents Sea leads to sea ice formation and can advect additional sea ice into the region. In the summer, sea ice melt and surface heating form a stratified meltwater layer in the upper water column. By autumn, the beginnings of sea ice formation, cooling, and turbulence lead to water column mixing. This overturning of the water column continues throughout the polar night and into spring. Dense water formation on the Barents Sea shelf enters the Arctic Basin through deep water plumes along the continental shelf (Rudels et al., 2000).

On the western coast of Svalbard, the West Spitsbergen Current brings AW into the Eurasian Basin. This current continues parallel along the Barents Sea shelf break and past Franz Josef Land in the east. This AW shows a distinct seasonality, with warmer temperatures in autumn and colder temperatures in early spring (Pérez-Hernández et al., 2019). As AW enters the Arctic Basin, it begins to cool and sinks below PW, forming an AW core at around 300 m depth in the water column north of Svalbard. As mixing occurs between AW and PW, continued temperature losses lead to the formation of modified Atlantic Water (mAW) below the pycnocline and AW core. As this water continues to cool below 0°C and sinks, typically below 1000 m, it forms Eurasian Basin Deep Water (EBDW). In addition, extensions of the West Spitsbergen Current flowing onto the northern Barents Sea shelf (Lundesgaard et al., 2022) can form warm Polar Water (wPW). This wPW is not as salty as AW yet warmer than PW, and can be found in deeper depths of the northern Barents Sea shelf or at the surface during summer stratification.

2.2 Field Sampling

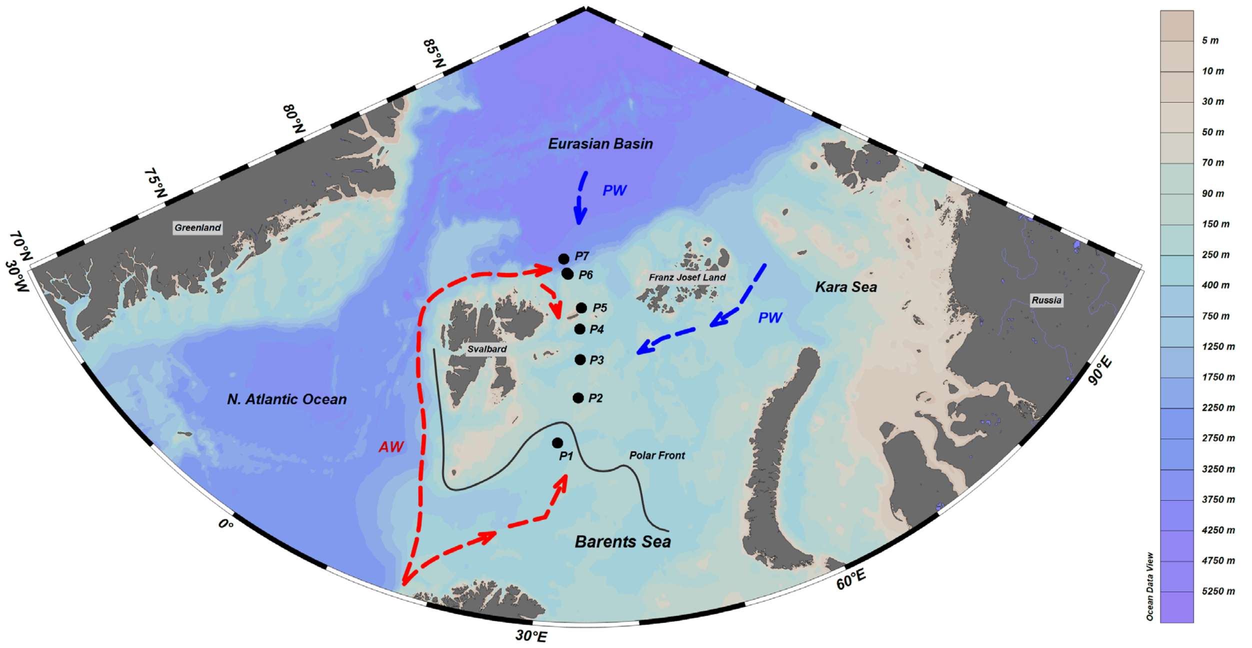

Figure 1: Map of sampling locations (stations P1-P7) in the northern Barents Sea region. A solid black line indicates the approximate location of the Polar Front, while the dashed colored arrows show a simplified water mass scheme and current direction, with Atlantic Water (AW) in red and Polar Water (PW) in blue. The color bar indicates water depth. Map created with Ocean Data View (Schlitzer 2021).

All samples were collected on a south-north transect in the northern Barents Sea and Nansen Basin (76 – 83°N) on two cruises, Q1 from March 2-24, 2021 (hereafter referred to as late winter), and Q2 from April 27 - May 20, 2021 (hereafter referred to as spring), on R/V *Kronprins Haakon* as part of The Nansen Legacy project (Fig. 1). Seawater samples for Hg were taken at seven stations at 8 depths down to 500 m depth using Teflon-coated GOFLO bottles attached sequentially to a 600 m nonmetallic wire. At depths deeper than 500 m, Hg samples were collected with 10 L Niskin bottles mounted to a rosette. Upon retrieval, GOFLO bottles were transported immediately to a custom-made clean lab onboard. THg samples were collected unfiltered into pre-cleaned (Cutter et al., 2017) 40 mL borosilicate glass bottles with PTFE-lined caps with no headspace and kept unpreserved. MeHg samples were collected unfiltered into brand new 125 or 250 mL PET bottles and were acidified under a Class 100 clean air laminar flow hood to 0.4% v/v with double-distilled HCl. Upon acidification, dimethylmercury (DMHg) converts quantitatively to monomethylmercury (MMHg) (Black et al., 2009); as a result, the sum of MMHg and DMHg is measured as total methylated mercury (MeHg). All Hg samples were double-bagged and stored in the dark at 4°C until analysis. Field blanks for THg were collected by bringing laboratory MilliQ onboard and subsampling at the time of field sampling into precleaned borosilicate bottles and treated identically to seawater samples. However, as we could not guarantee trace metal clean Niskin bottles for samples collected below 500 m, these data are reported (SI Fig. 1) but not included in subsequent statistical processing when noted.

Under ice water (UIW) was collected using a handheld 10 L Niskin bottle lowered into a hole cut into the sea ice at stations P4, P6, and P7 on both cruises. UIW was collected directly from the Niskin similar to the other seawater samples. Sea ice was collected at two stations, P4 and P7, using a 9 cm diameter ice corer (Kovacs Enterprises, Inc., USA), bagged whole and taken directly onboard into a -20°C cold lab. The bottom 10 cm of the ice core was cut using a handheld carbon steel saw. Approximately 3 mm of ice was shaved off from all sides of the ice section with a ceramic knife to remove any potential contamination before being double bagged and melted at room temperature. One frost flower sample was collected in late winter using plastic equipment and melted at 4°C. After melting, all samples were decanted into precleaned 40 mL borosilicate glass bottles and 125 or 250 mL PET bottles and stored in the dark at 4°C until analysis.

2.3 Mercury Analysis

The concentration of THg in the samples was measured by cold vapor atomic fluorescence spectroscopy (CVAFS) according to USEPA Method 1631 at the Mediterranean Institute of Oceanography (MIO) using a custom-made single gold trap setup described elsewhere (Heimbürger et al., 2015, Kohler et al., 2022a), within one year after sampling. As samples were unfiltered to reduce contamination risk from filtration equipment, THg concentration includes both particulate and dissolved species of Hg. The THg concentration in all samples was calculated from a 6-point calibration curve traceable to NIST 3133 (National Institute of Standards and Technology) standard reference material in previously purged, Hg-free seawater. Standard bracketing of samples with a NIST 3133 matrix spike were used to correct for eventual instrument signal drift and ensure ongoing precision and recovery. Aliquots of certified reference materials

ORMS-5 (Research Council of Canada) and ERM-CA400 (European Reference Materials) were spiked into previously purged Hg-free seawater matrix with recoveries of 93 ± 2% and 125 ± 4%, respectively. Selected seawater samples run in triplicate from both cruises had an average standard deviation of 0.05 pmol L^{-1}. Field blanks of MilliQ water were measured for THg for both late winter (0.31 ± 0.02 pmol L^{-1}, n = 5) and spring (0.23 ± 0.02 pmol L^{-1}, n = 3) cruises. As MilliQ water can potentially contain traces of Hg, we concluded that there was no significant contamination affecting our THg measurements.

The MeHg concentrations in seawater samples was measured using the isotope dilution (ID) technique via gas chromatography (GC) – sector field ICP-MS (GC-SF-ICP-MS) at MIO within one year after sampling (Heimbürger et al., 2015). Briefly, approximately 125 mL of seawater sample was spiked with enriched isotopes of $i^{199}Hg$ and $MM^{201}Hg$ (ISC Science) and equilibrated for 15 minutes. Samples were then adjusted to pH 3.9 using a sodium acetate buffer solution (ULTREX® II Ultrapure Reagent, J.T. Baker, USA) and NH_3 (ULTREX® II Ultrapure Reagent, J.T. Baker, USA). A fresh aliquot of 1% sodium tetrapropylborate solution (Merseburger Spezialchemikalien) and 150 µL of isooctane (Sigma Aldrich) were added to derivatize and preconcentrate Hg species. Samples were sealed and shaken for 15 minutes before the organic extract was transferred to GC vials for analysis on a coupled GC (THERMO GC 1300 with GC220 transfer module) SF-ICP-MS (Thermo Element XR) system. Ultra-trace clean techniques and coupling to a high resolution ICP-MS allows a detection limit of 2 fmol L^{-1} and a limit of quantitation of 7 fmol L^{-1} (LOQ = 3.3*LOD). Selected seawater samples run in duplicate from both cruises had an average standard deviation of 7 fmol L^{-1}. The $MM^{201}Hg$ spike concentration used to calculate the sample MeHg concentrations had an accuracy of 94.4 ± 8.4%. The accuracy of our spike was determined using reverse isotope dilution using the Brooks Rand MMHgCl standard, traceable to NIST1641E.

2.4 Additional Data and Parameters

Water temperature and salinity were recorded on a Seabird SBE 9 CTD unit attached to a rosette. Quality controlled temperature, salinity, sea ice concentration, nutrients, chlorophyll *a*, particulate organic carbon, nutrients, and phytoplankton abundance data for all seasonal cruises were retrieved from the Norwegian Marine Data Centre and the Norwegian Polar Institute (Gerland 2022, Ludvigsen 2022, Reigstad 2022, Søreide 2022, Steer and Divine 2022, Marquardt 2022b, 2022c, 2022d, 2022e, Müller 2023a, 2023b, 2023c, 2023d, Chierici et al. 2021a, 2021b, Jones et al., 2022a, 2022b, Vader 2022, Assmy 2022a, 2022b). Part of the late winter MeHg data (station average, upper 400 m only) presented in this analysis was previously published in the bottom image in Fig. 6 in Dietz et al., 2022. Flow cytometry, bacterial community analysis, and dissolved organic matter analysis details are presented in the Supplementary Information. Latitude and longitude coordinates for CTD stations differ slightly from GOFLO casts due to ship drift. Conservative temperature (Θ), absolute salinity (S_A), and potential density anomaly (σ_θ) were calculated in Ocean Data View. Water mass definitions were assigned based on the most recent report from the Nansen Legacy project for the northern Barents Sea (Sundfjord et al., 2020).

Statistical processing was performed for data above 500 m depth in Minitab software. Spearman rank correlation coefficients were calculated using a 95% CI with significant p-value < 0.05. Data selected for Student's t-test were log transformed for non-normal data distributions prior to evaluation using a 95% CI with significant p-value < 0.05. Log-log regression was performed on selected environmental variables with significance evaluated by F-test with a 95% CI and significant p-value < 0.05. Selected environmental parameters were chosen for Principal Component Analysis, where data is standardized prior to dimension reduction and plotted orthogonally as loadings plots for the first two principal components.

3 Results & Discussion

3.1 Hydrography & sea ice

In general, all stations in the northern Barents Sea showed both similarities and differences in water mass distributions (SI Figs. 2 & 3) in both late winter and spring, with changes influenced by sea ice coverage or temperature shifts (Jones et al., 2023, Van Engeland et al., 2023). In the late winter and spring sampling periods, station P1 south of the polar front had a mAW signature, with S_A greater than 35.06 g kg^{-1} and $\Theta > 0$°C. Stations P2, P3, and P4, all north of the polar front, had PW ($\Theta < 0$°C, $\sigma_\theta < 27.97$ kg m^{-3}) in surface waters and wPW ($\Theta > 0$°C, $S_A < 35.06$ g kg^{-1}) in deeper waters extending to the bottom. A deepening of PW in spring at stations P2-P5 could suggest rapidly changing sea ice conditions (SI Fig. 4), with small increases in salinity indicating refreezing and brine rejection. Station P5 had low temperatures, with PW throughout the entire water column in both seasons. Stations P6 and P7 intersect the West Spitsbergen Current, with PW and wPW in surface waters extending until approximately 200 m depth, where both mAW and AW ($\Theta > 2$°C, $S_A > 35.06$ g kg^{-1}) extends down to about 500 m. In waters below 500 m, mAW persists until about 800 m depth and EBDW ($\Theta < 0$°C, $S_A > 35.06$ g kg^{-1}) fills the Nansen Basin. At the time of sampling in late winter, first-year sea ice covered all stations except for P1 (Marquardt et al., 2023a). Some sea ice changes were observed during sampling (SI Fig. 4), but in general most stations were covered by close drift ice. Minor changes in ice coverage occurred before sampling for shelf stations, while P6 and P7 showed significant variations in ice coverage. However, by the end of the late winter campaign, P6 and P7 were also covered by close drift ice. Shelf stations P2-P5 showed dynamic ice conditions in between the late winter and spring cruises, while P6 and P7 were covered by slightly older sea ice in spring (Marquardt et al., 2023a).

3.2 THg and MeHg distributions in the water column during late winter and spring

THg concentrations in late winter (Fig. 2, top left) in the northern Barents Sea and Nansen Basin were on average 0.56 ± 0.17 pmol L^{-1} (Table 1). In spring (Fig. 2, top right), THg concentrations in the northern Barents Sea and Nansen Basin were on average 0.69 ± 0.24 pmol L^{-1} (n = 67, ± 1SD, range: 0.46 - 2.37 pmol L^{-1}). In the upper 500 m, our average THg concentrations on the spring cruise (0.64 ± 0.09 pmol L^{-1}, n = 56) were significantly higher (log transformed, Student's t-test, $p < 0.05$) compared to late winter (0.53 ± 0.07 pmol L^{-1}, n = 51). On the shelf, our THg concentrations in both late winter and spring (Table 1) are similar to THg concentrations in the southern Barents Sea Opening (0.43 ± 0.14 pmol L^{-1}) (Petrova et al., 2020) and comparable to previous expeditions in this area (0.63 ± 0.19 pmol L^{-1} in summer, and 0.46 ± 0.07 pmol L^{-1} in early winter) (Kohler et al., 2022a). In late winter, shelf stations P1 - P5 exhibited relatively constant THg concentration profiles with depth, similar to early winter 2019 (Kohler et al., 2022a) while spring vertical THg profiles are similar to observed THg profiles in summer 2019 (Kohler et al., 2022a), with enrichments in surface waters < 50 m.

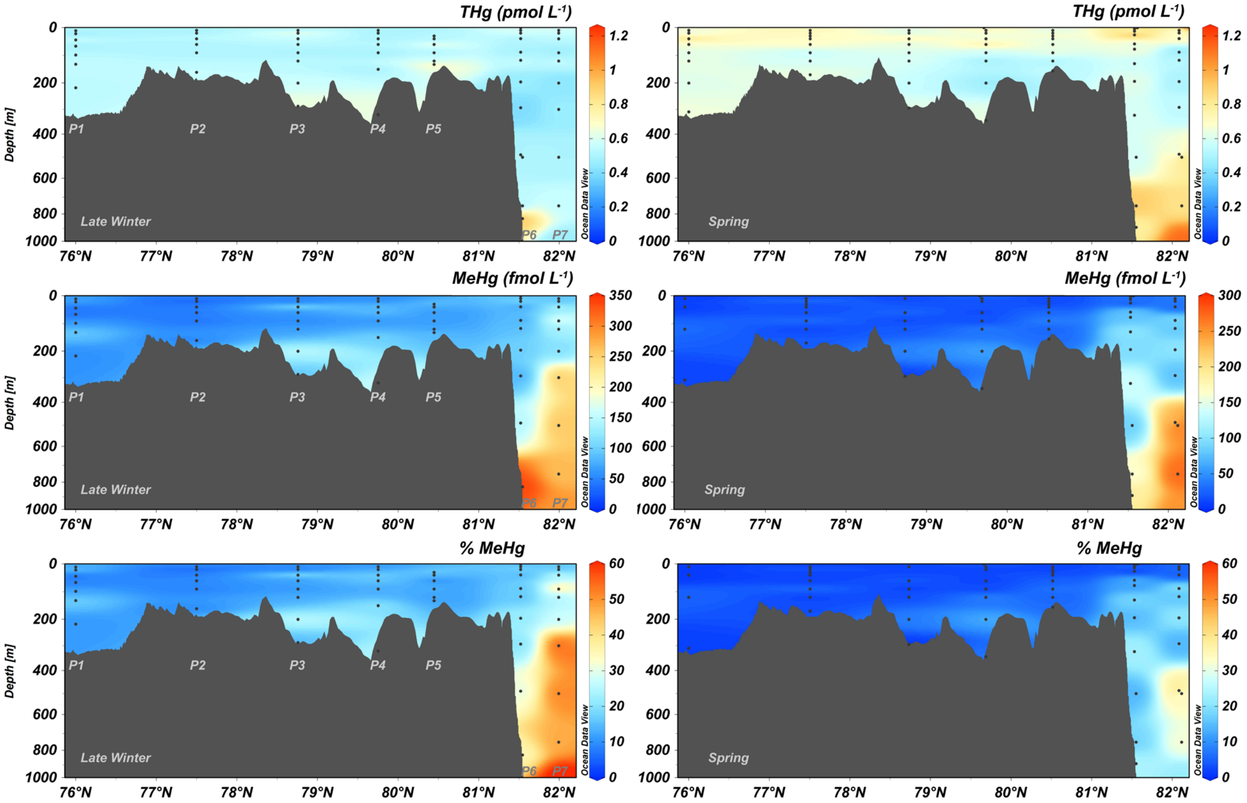

Figure 2: THg concentrations (top, pmol L^{-1}), MeHg concentrations (middle, fmol L^{-1}), and % MeHg as THg (bottom) along the shelf-basin transect in the northern Barents Sea during late winter (left) and spring (right) in 2021. The maximum plotted THg concentration range is 1.25 pmol L^{-1}. Depths where MeHg concentration < LOQ (7 fmol L^{-1}) have been removed from the visualization. The x-axis displays latitude and the nonlinear y-axis is in units of depth (m). Transect created with Ocean Data View (Schlitzer 2021).

MeHg concentrations (Table 1, Fig. 2 middle left) along the entire transect during late winter were 112 ± 76 fmol L^{-1} (n = 58, ± 1SD). At station P6 and P7, MeHg concentrations were lowest near the surface and directly below the ice (UIW = 59 ± 11 fmol L^{-1}, n = 2). At P7, MeHg concentrations greater than 250 fmol L^{-1} began at 300 m depth in the AW core of the West Spitsbergen Current. By the spring cruise, MeHg concentrations along the entire transect were 69 ± 75 fmol L^{-1} (n = 60, ± 1SD) (Fig. 2, middle right) and covered a relatively large range (Table 1). In the upper 500 m, our average MeHg concentrations on the spring cruise (41 ± 39 fmol L^{-1}, n = 49) were significantly lower (log transformed, Student's t-test, $p < 0.05$) compared to late winter (85 ± 42 fmol L^{-1}, n = 51). Shelf stations in spring exhibited low MeHg concentrations in general (Table 1), with the lowest MeHg concentrations observed at P1 in mAW and some measurements below the LOQ of 7 fmol L^{-1}. Previous seasonal expeditions on the northern Barents Sea shelf showed similarly constant MeHg distributions with depth, albeit with slightly higher average MeHg concentrations (Kohler et al., 2022a). Our spring MeHg concentrations on the shelf however, are also lower than both the Barents Sea Opening (~ 60 ± 30 fmol L^{-1}) (Petrova et al., 2020) and among the lowest reported for the Arctic region (Jonsson et al., 2022a). Percent MeHg (%MeHg) in both seasons follows a similar distribution pattern as MeHg concentrations (Figure 2, bottom), with higher %MeHg observed in subsurface waters. In late winter, %MeHg is 20 ± 13% (n = 58) while spring %MeHg is 10 ± 10% (n = 60). Similar to MeHg, there is a significant difference in %MeHg in the upper 500 m (log transformed, Student's t-test, $p < 0.05$) between late winter (16 ± 9%, n = 51) and spring cruises (7 ± 8%, n = 49).

The highest THg concentrations for both late winter and spring were observed in deep waters of P6 and P7 between 500 - 1500 m depth and both maxima are observed 10 m from the bottom of the Nansen Basin (SI Fig. 1). Our unfiltered THg observations in basin waters in both late winter and spring are within the ranges reported in the central Arctic Ocean (Heimbürger et al., 2015, Wang et al., 2018, Agather et al., 2019, Jonsson et al., 2022b) and the Fram Strait (Petrova et al., 2020). Similarly, relatively high MeHg concentrations were observed in basin waters > 500 m (SI Fig. 1). These findings in late winter are similar to deep water MeHg concentrations observed in the Fram Strait (Petrova et al., 2020) and the central Arctic Ocean (Jonsson et al., 2022b). However, as we could not guarantee trace metal clean Niskin bottles for our deep water sampling (> 500 m), some caution is needed when interpreting these results.

Table 1: Average (± one standard deviation) and range of THg, MeHg, concentrations and % MeHg on both late winter and spring cruises for all water column samples, shelf stations (P1 - P5), basin stations (P6, P7), under ice water (UIW), ice cores, and frost flowers (FF).

	Total Hg (pmol L^{-1})					**Methylated Hg (fmol L^{-1})**					
	Late winter		**Spring**			**Late winter**			**Spring**		
	Average ± 1SD	**Range**	**Average ± 1SD**	**Range**		**Average ± 1SD**	**Range**	**% MeHg as THg**	**Average ± 1SD**	**Range**	**% MeHg as THg**
All water column data	0.56 ± 0.17 (n = 60)	0.40 - 1.61	0.69 ± 0.24	0.46 - 2.37 (n = 67)	**All water column data**	112 ± 76 (n =58)	20 - 340	20 ± 13	69 ± 75 (n = 60)	< 7 - 288	10 ± 10
Upper 500 m only	0.53 ± 0.07 (n = 51)	0.40 - 0.77	0.64 ± 0.09	0.46 - 0.94 (n = 56)	**Upper 500 m only**	85 ± 42 (n = 51)	20 - 254	16 ± 9	41 ± 39 (n = 49)	<7 - 204	7 ± 8
Shelf (P1-P5) all depths	0.54 ± 0.07 (n = 34)	0.47 - 0.77	0.64 ± 0.08	0.46 - 0.84 (n = 40)	**Shelf (P1-P5) all depths**	71 ± 32 (n = 34)	20 - 161	13 ± 5	23 ± 13 (n = 33)	< 7 - 60	4 ± 3
Basin (P6, P7) all depths	0.59 ± 0.24 (n = 26)	0.40 - 1.61	0.76 ± 0.36	0.47 - 2.37 (n = 27)	**Basin (P6, P7) all depths**	171 ± 82 (n = 24)	72 - 340	30 ± 15	127 ± 79 (n = 27)	21 - 288	18 ± 10
UIW	0.58 ± 0.02 (n = 3)	0.56 - 0.60	1.00 ± 0.30	0.73 - 1.32 (n = 3)	**UIW**	59 ± 11 (n =2)	50 - 67	10 ± 2	36 ± 17 (n = 3)	26 - 55	4 ± 1
Ice core	0.27 ± 0.10 (n = 2)	0.20 - 0.34	1.83 ± 0.40	1.55 - 2.12 (n = 2)	**Ice core**	n/a			n/a		
FF	24.03 (n = 1)		n/a		**FF**	n/a			n/a		

To understand how changes in physical oceanography may affect our distributions of both THg and MeHg species, we averaged Hg concentrations by water mass in the upper 500 m, visualized in Fig. 3 and summarized in Table S1. Significant differences (log transformed, Student's t-test, $p < 0.05$) for both THg and MeHg concentrations in late winter and spring were observed for PW. A significant difference in THg concentrations was also observed for mAW, which was mainly observed in waters at station P1. No difference was observed for MeHg in mAW, although we assumed this is mainly due to local MeHg concentration differences in surface mAW at station P1 and subsurface mAW at stations P6 and P7. No statistically significant differences were observed for THg nor MeHg concentrations in wPW, which comprised only subsurface and bottom waters at our stations (Van Engeland et al., 2023). As PW comprises most of our shelf stations and surface waters at P6 and P7, our observed changes in THg concentrations are best explained by external inputs to surface waters such as atmospheric deposition or ice melt instead of changes in water mass. In addition, our general transect (Fig. 2) and insignificant differences in wPW (Table 2) do not suggest major inputs of benthic THg nor MeHg during this time period. We also cannot rule out potential concentration differences in individual water parcels between sampling periods, but we infer that our observed THg profiles and differences in THg concentrations in spring reflect seasonal THg inputs to surface waters. Similarly, we hypothesize our lower MeHg concentrations in spring are driven by internal biogeochemical processes rather than external inputs and/or water masses.

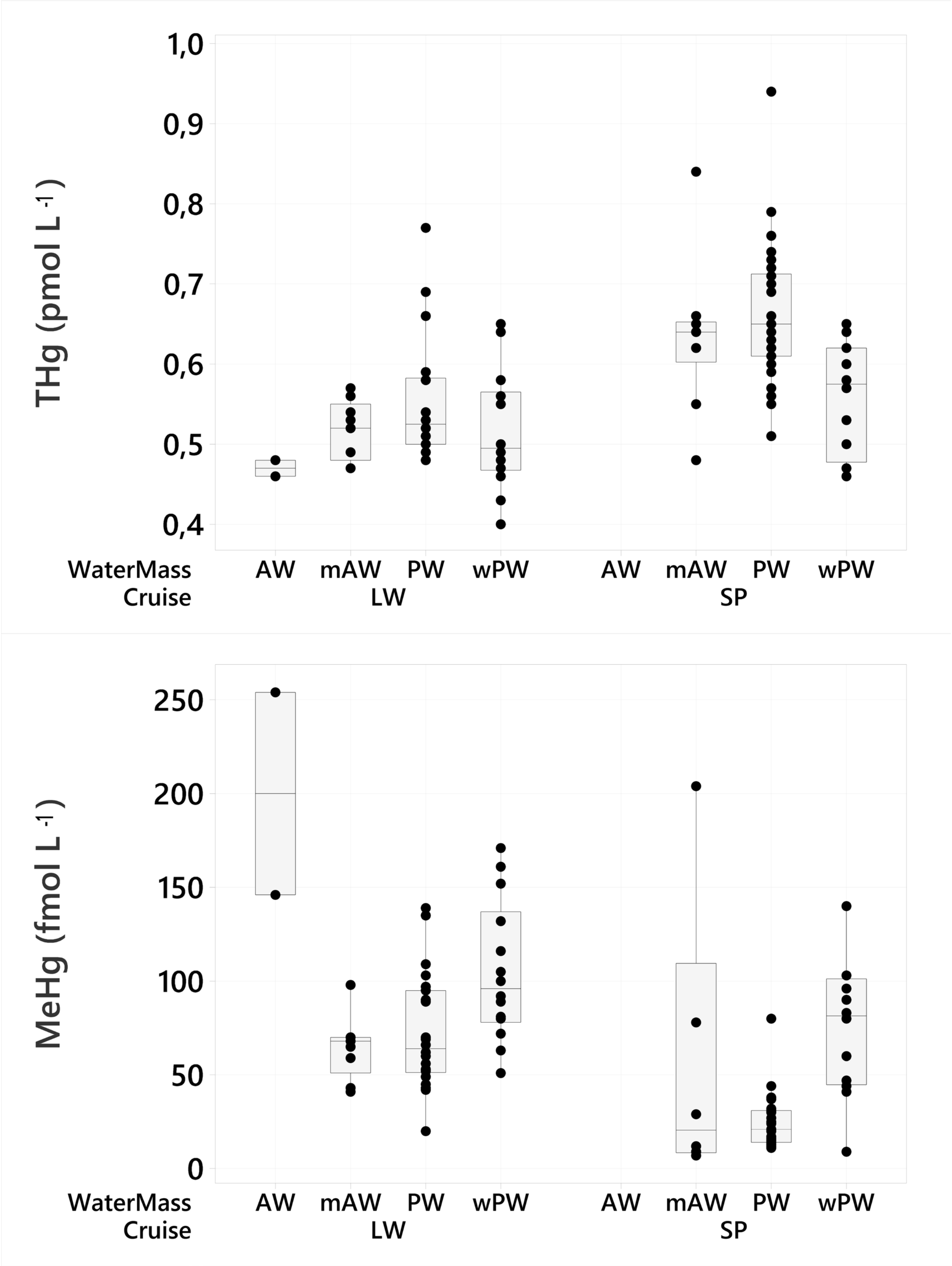
THg (pmol L-1)
1,0
0,9
0,8
0,7
0,6
0,5
0,4
WaterMass
Cruise
AW
mAW
PW
wPW
LW
AW
mAW
PW
wPW
SP
MeHg (fmol L-1)
250
200
150
100
50
0
WaterMass
Cruise
AW
mAW
PW
wPW
LW
AW
mAW
PW
wPW
SP

Figure 3: THg (top) and MeHg (bottom) concentrations averaged for water masses in both late winter (LW) and spring (SP) in the northern Barents Sea in 2021. Water masses are Atlantic Water (AW), modified Atlantic Water (mAW), Polar Water (PW), and warm Polar Water (wPW). Box plots display median (± IQR) and individual data points for each water mass. For averages and sample sizes, see Table S1.

3.3 Seasonal inputs of THg to surface waters

Elevated THg in surface waters in spring could suggest inputs from AMDEs or sea ice processes, where changing sea ice conditions facilitate atmospheric deposition to surface waters. Although much of the AMDE-derived Hg is photochemically re-emitted back to the atmosphere from the cryosphere during the summer (Dastoor et al., 2022), a temporary enrichment could exist during spring. Under ice water (UIW) taken at stations P4, P6 and P7, in late winter was 0.58 ± 0.02 pmol L^{-1} ($n = 3$), similar to the remaining THg levels in the water column. However, the bottom 10 cm of ice cores taken at P4 and P7 had low THg concentrations, with values of only 0.34 pmol L^{-1} and 0.20 pmol L^{-1}, respectively. As sea ice appeared to both melt and freeze in between our two sampling periods (SI Fig. 4), it is plausible that dynamic melt and freeze processes facilitated additional THg to surface waters. However, changes in integrated THg in seawater (upper 100 m) do not show a correlation with the average fraction of open water (SI Fig. 5). We suspect that the heterogeneity in sea ice and snow may deliver variable amounts of Hg to surface waters, as the sea ice covering our stations during the two seasonal cruises have different origins and drift patterns (Marquardt et al., 2023a). Previous studies in the Arctic found higher concentrations and a wide range of THg (range: 0.089 - 60.8 pmol L^{-1}) in both first year ice and multiyear ice compared to seawater (Chaulk et al., 2011, Beattie et al., 2014, Schartup et al., 2020, Jonsson et al., 2022b). Although we measured low THg concentrations in the bottom sea ice in late winter, THg can vary by up to an order of magnitude throughout the core, with highest concentrations near the sea ice-atmosphere interface (Beattie et al., 2014). As sea ice drifts and snow and ice melts between cruise samplings (SI Fig. 4), these reservoirs could supply additional Hg to surface seawater (Huang et al., 2023). Furthermore, any leads in the ice pack during these changing ice conditions could also facilitate direct atmospheric deposition of AMDEs to surface seawater or deposit additional Hg to the cryosphere (Moore et al., 2014).

Refreezing also results in the rejection of brine between sampling periods (SI Fig. 4), with brine THg concentrations potentially up to 355 pmol L^{-1} (Chaulk et al., 2011). Although we did not measure brine directly, a frost flower formed from brine expulsion in late winter had a concentration of 24 pmol L^{-1} ($n = 1$). By spring, UIW concentrations were 1.00 ± 0.30 pmol L^{-1} ($n = 3$), and higher than the average concentration for the remaining water column. Likewise, in sea ice, the THg concentration in the bottom 10 cm of ice cores taken at P4 and P7 were higher in spring, with values of 1.55 pmol L^{-1} and 2.12 pmol L^{-1}, respectively. Spring THg concentrations in the bottom of ice cores are higher compared to our late winter observations, which contrasts with a seasonal study in Antarctica (Nerentorp Mastromonaco et al., 2016). Local melt and freeze processes, downward brine movement, and varying sea ice advection are most likely responsible for the differences observed in the two studies. However, seasonal increases in THg in the Antarctic water column from winter to spring were suggested to be a result of both atmospheric and sea ice processes (Nerentorp Mastromonaco et al., 2017). Consequently, we conclude that our observed seasonal THg water column concentrations most likely reflect similar seasonal inputs and processes.

3.4 Potential uptake of THg by the spring bloom

Increased THg concentrations in surface waters and sea ice in spring could also be driven by the onset of primary productivity (SI Fig. 6). Development of ice algae during the spring bloom can take up THg from brine and seawater (Burt et al., 2013), explaining our increased THg concentrations in the bottom of sea ice. In the water column, Spearman's rank correlation analysis in spring indicated significant positive relationships between THg, particulate organic carbon (POC) and chlorophyll *a* (Table S3). Additionally, elevated chlorophyll *a,* pico-, nano-, and microphytoplankton in surface waters were observed in spring, indicating recent development of the phytoplankton spring bloom (SI Figs. 6 & 9). Log-log regression models between THg, POC, and chlorophyll *a* concentrations in the upper 500 m for all stations in spring (Fig. 4A, 4C) showed a positive and statistically significant relationship (F-test, $p < 0.05$). Compared to late winter, this analysis suggests that THg is more associated with the particulate phase. If we assume POC as a proxy for total particulate matter and a constant partition coefficient K_d to calculate dissolved Hg (dHg) and particulate Hg (pHg) (SI Equations 3 and 4), this also indicates a greater percentage of pHg in spring when compared to late winter. A strong positive Spearman rank correlation also exists between POC and chlorophyll *a* (Table S3, $p < 0.05$), suggesting that the positive correlation of THg with both of these biological indicators may suggest adsorption and/or uptake of Hg species to primary producers during the spring bloom (Burt et al., 2014, Luengen and Flegal 2009).

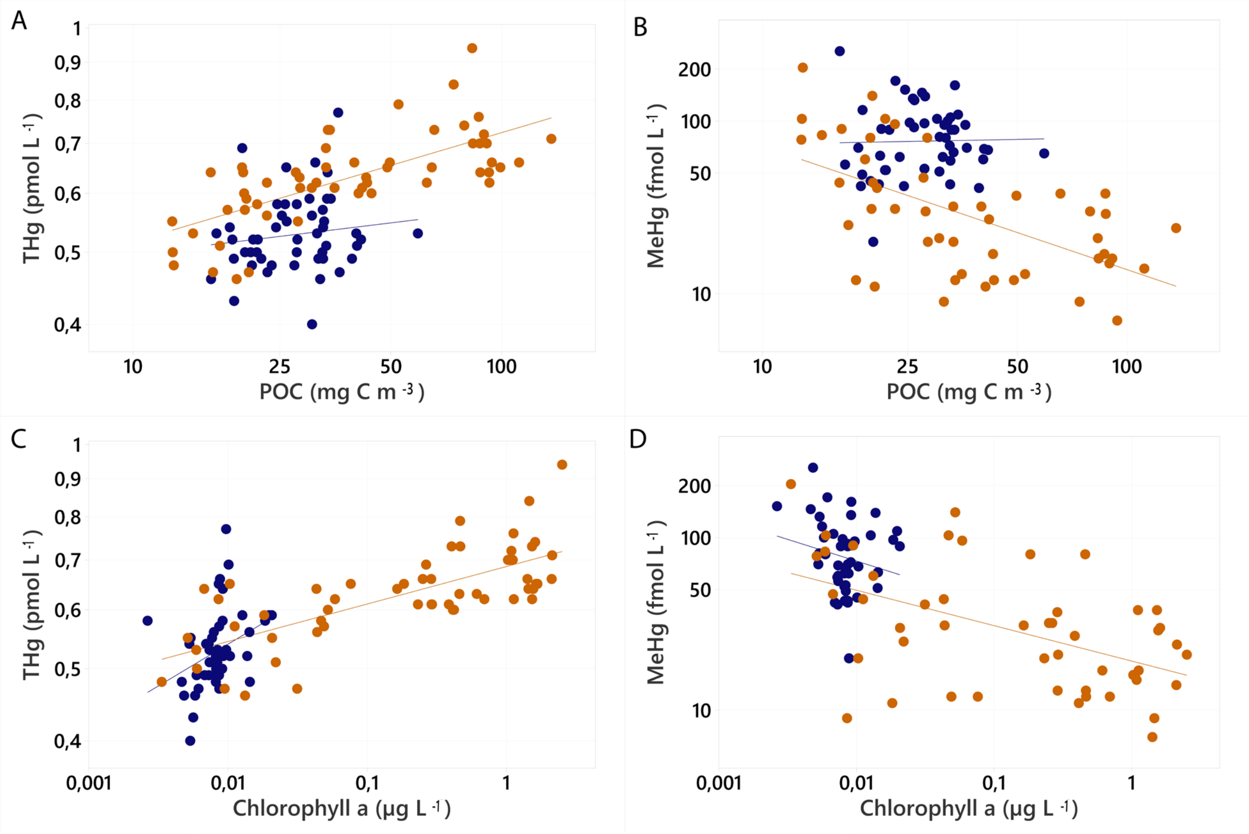

Figure 4: Log scale scatterplots with log-log regressions of THg (left) and MeHg (right) concentrations against POC (top) and chlorophyll *a* (bottom) concentrations in the upper 500 m for both late winter (blue) and spring (orange) in the northern Barents Sea in 2021.

However, it is important to note that higher THg concentrations in spring suggest that seasonal inputs increase both pHg and dHg concentrations, with a significant fraction of THg in the dissolved phase. While our THg relationships to biological parameters during the spring bloom suggests that THg is either taken up into primary producers by diffusion or adsorbed to cell surfaces, the remaining dHg in the water column can also be complexed by extracellular algal exudates (Cossart et al., 2022). In the dissolved phase, Hg shows strong affinity to DOM and especially to reduced sulfur ligands (Ravichandran 2004). Indeed, we saw increased relative intensities of dissolved organic sulfur compounds (CHOS) in surface waters in both sampling periods compared to deeper waters (SI Fig. 7), most likely released by phytoplankton. These biologically driven processes, such as uptake by phytoplankton and organic matter complexation, could keep THg sourced from the atmosphere or sea ice in surface waters as well as facilitate transformations of Hg species.

3.5 MeHg dynamics in late winter and spring

Significant differences in MeHg concentrations from late winter to spring can be driven by several biogeochemical processes. As our spring MeHg concentrations showed a significant decline compared to late winter, the collective sinks of MeHg in the water column outweigh MeHg sources. Potential MeHg sinks to consider are photodemethylation, particle scavenging of MMHg, atmospheric evasion of DMHg, and dark demethylation processes. To systematically evaluate the contribution of each of these potential sinks, we used both literature and field data to calculate the percentage contribution to the observed difference in the upper 100 m. It is important to note that our observed differences in MeHg are net values, which can lead to high uncertainty when estimating the contribution from various sources and sinks.

We integrated the water column for MeHg for each station to calculate the rate of change per day, called ΔMeHg (Kohler et al., 2022a) for each station using the following equation:

$$\Delta MeHg = \left(\int_0^z [MeHg]_{SP} dz - \int_0^z [MeHg]_{LW} dz\right) / dt$$

Here, we used the trapezoidal integration method to calculate from 0 to 100 m depth, where z = depth, SP = spring, and LW = late winter, and t = time in days between sampling of each station. The total integrated pools are summarized in Table S4. All stations show a net decline, or loss, in the integrated pool from late winter to spring with an average of -81 ± 36 pmol m^{-2} d^{-1} (n = 7), demonstrating that sinks outweigh sources for observed change in MeHg concentrations.

Our measured declines of MeHg pools by spring could be due to increased photodemethylation during the transition to polar day. However, both lower water temperatures and the presence and thickness of snow and sea ice hinder MeHg photodemethylation (Point et al., 2009). Previous estimates in the Arctic Ocean suggest photodemethylation rates of 0.04 d^{-1} (Lehnherr et al., 2011) and 0.0082 d^{-1} (Zhang et al., 2020) at the sea surface. Assuming first-order kinetics and using ΔMeHg, our calculated rate constant for our seven stations in the upper 100 m between late winter to spring is an average MeHg loss of 0.021 ± 0.013 d^{-1} (n = 7). This loss, although a net loss and not directly comparable, agrees well with the estimated photodemethylation rate constants; however, the photodemethylation rate would be attenuated with depth and dependent on available light. To estimate the percentage of the MeHg pool potentially degraded due to photodemethylation at each station, we used photosynthetically active radiation (PAR) approximated to 15 E m^{-2} d^{-1} between the months of March and May 2021 (SI Fig. 8) and rate constant from Arctic waters of 0.001 m^2 E^{-1} when expressed to solar irradiance (Lehnherr et al., 2011). After accounting for the fraction of open water (with a simple assumption of zero transmittance through snow-covered sea ice) and attenuation of PAR with depth (Table S6), our calculations suggest that photodemethylation can only account for 5 ± 4% of our observed ΔMeHg in the upper 100 m (Fig. 5). The highest percentage of photodemethylation (11%) is observed at station P1 due to no sea ice coverage. This calculation carries a high uncertainty due to additional variables we could not account for, such as the partial transmittance of light through sea ice, enhanced or inhibited photodemethylation in the presence of DOM, and scattering and absorption of light by both particles and DOM. Nevertheless, potential photodemethylation plays a relatively small role compared to our observed changes in MeHg pools.

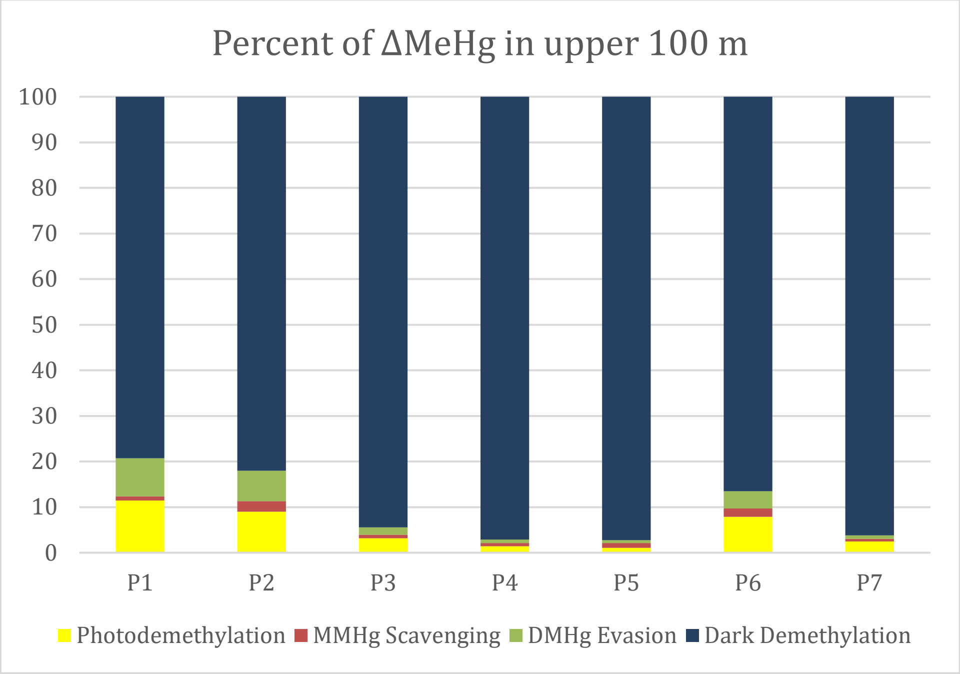

Figure 5: Percent contribution of selected processes influencing the change in MeHg pools, ΔMeHg, between late winter and spring. Photodemethylation is in yellow, MMHg particle scavenging in red, DMHg evasion in green, and dark demethylation (all other unaccounted for processes) in dark blue.

Particulate scavenging could also potentially serve to transport particle-bound MMHg (pMMHg) to deeper waters. As the total amount of sinking particles, including POC, are low in late winter waters due to the lack of biological productivity (Dybwad et al., 2022), we could assume that scavenging of pMMHg is negligible. Furthermore, a previous study has estimated that only 4% of pHg is pMMHg, which might be overestimated due to several samples below the detection limit (Agather et al., 2019). Additionally, observed POC fluxes across our transect in late winter were low at 27 ± 9 mg C m^{-2} d^{-1} (Bodur et al., 2023) with no flux attenuation, suggesting minimal vertical pHg transport. For comparison, POC fluxes in spring were 178 ± 199 mg C m^{-2} d^{-1} (Bodur et al., 2023). While we only measured MeHg and do not know exactly when primary production began to develop, we made several assumptions to attempt to determine the contribution of pMMHg scavenging to ΔMeHg (Table S6), with an estimate of 1 ± 1% of ΔMeHg (Fig. 5).

In surface waters, shifts in ice coverage could lead to evasion of DMHg trapped below the ice and help explain lower MeHg in surface waters during spring. In UIW, MeHg concentrations were 59 ± 11 fmol L^{-1} (n = 3) in late winter and 36 ± 16 fmol L^{-1} (n = 3) in spring. As our average UIW concentrations of MeHg in spring were lower than in late winter, it is possible DMHg has evaded to the atmosphere during melting and freezing, or DMHg has built up in the overlying sea ice (Schartup et al., 2020). Previous studies have emphasized the importance of the evasion of DMHg from Arctic waters (Baya et al., 2015, Soerensen et al., 2016) but recent studies of DMHg in sea ice and surface seawater (Agather et al., 2019, Jonsson et al., 2022) suggest a relatively modest evasion rate. Although we did not measure DMHg, we expect a large proportion of our surface MeHg concentrations to consist of MMHg, similar to other Arctic Ocean studies (Baya et al., 2015, Agather et al., 2019, Jonsson et al., 2022b). We attempted to quantify the amount of DMHg evasion during our transition to spring with additional limitations and assumptions (Table S6), with atmospheric evasion making up only 3 ± 3% of ΔMeHg (Fig. 5). As this estimate is a gross value and does not account for atmospheric re-deposition of MMHg, it may be overestimated.

Water mass distribution along our transect did not change drastically from late winter to spring (Van Engeland et al., 2023), suggesting relatively minimal importance of advection of lower concentration MeHg waters in the upper 100 m. However, station P6 and P7 do intercept the West Spitsbergen Current, with slight shifts from wPW to PW in spring (Van Engeland et al., 2023). MeHg concentrations in PW are lower than wPW in late winter (One-way ANOVA with Tukey's test, $p < 0.05$), and could contribute to the observed ΔMeHg. Nevertheless, PW is significantly different between the two cruises, so for the sake of simplicity we have assumed advection plays a negligible role in explaining our observed ΔMeHg.

The importance of dark demethylation processes in unfiltered waters has been highlighted in previous studies using spiked stable Hg isotopes to measure demethylation rates (Lehnherr et al., 2011, Monperrus et al., 2007). In addition, the recent MeHg annual budget for the East Siberian Sea attributed approximately 50% of potential MeHg sinks to gross dark demethylation (Kim et al., 2020b). Consequently, we attribute the remaining ΔMeHg observed (90 ± 8%, Fig. 5) as dark demethylation processes and hypothesize that they are mainly driven by biological activity.

3.6 Biotic demethylation of MeHg

As POC fluxes were low in late winter (Bodur et al., 2023), it is likely that there is no substantial in situ biotic Hg methylation occurring throughout the water column. Additionally, despite a higher concentration of THg by spring, both MeHg concentrations and % MeHg have decreased (Fig. 2), suggesting methylation processes were dominated by demethylation processes. However, the increase in phytoplankton abundance by orders of magnitude in surface waters along the transect in spring could support biotic transformations of Hg species (SI Fig. 6). Upon development of the phytoplankton bloom, we observed that diatoms, particularly species of the genus *Thalassiosira*, had the highest relative abundance in the upper 90 m at five out of seven stations along our transect (SI Fig. 9). Our regression analysis (Fig. 4) supports the hypothesis that THg is indeed potentially taken up by primary producers. Unlike THg, however, MeHg has significant negative relationships with both POC and chlorophyll *a* in spring (Fig. 4B, 4D, F-test, $p < 0.05$), supporting declining MeHg concentrations in association with biological particles. As diatoms and other marine phytoplankton passively take up MMHg (Mason et al., 1996, Lee and Fisher 2016), we hypothesize that our observed MeHg losses in surface waters could be due to phytoplankton uptake and subsequent demethylation. This hypothesis is further supported by relatively low contributions of the other MeHg sinks in surface waters (Fig. 5) and possible biological demethylation mechanisms identified in literature. Previous research has observed reduction of inorganic Hg^{II} to Hg^0 in the diatom *Thalassiosira weissflogii* (Morelli et al., 2009) while the green alga *Chlamydomonas reinhardii* was demonstrated to demethylate MMHg (Bravo et al., 2014). Another study in a freshwater lake has shown that demethylation of intracellular MMHg correlated positively with diatom abundance (Cossart et al., 2021). Recently, a study suggested that phytoplankton can intracellularly demethylate MeHg through the production of reactive oxygen species (Liang et al., 2023).

This MMHg uptake during the onset of the Arctic spring bloom could potentially facilitate the seasonal bioaccumulation of MMHg by higher trophic level organisms throughout the summer. A previous study in an Arctic lake observed decreasing MeHg levels in water from winter to spring, yet saw a seasonal increase in MeHg concentrations in freshwater zooplankton (Varty et al., 2021). Furthermore, another winter to spring increase of MeHg concentrations in zooplankton was observed in waters of the Canadian Arctic Archipelago (Pućko et al., 2014). While other mechanisms like zooplankton grazing activity or direct methylation in the gut could explain their observed seasonal Hg biota concentrations (Pućko et al., 2014), we speculate that our seasonal changes of water column MeHg partly reflect a MMHg biomagnification pathway for higher trophic level organisms in the Arctic's productive spring and summer seasons.

Further studies on Hg methylation activity in specific marine phytoplankton species demonstrated that MeHg demethylation positively correlated with thiol concentrations in algal exudates (Li et al., 2022). We observed more elevated relative intensities of CHOS compounds in surface waters compared to deeper waters (SI Fig. 7). Dissolved CHOS compounds could facilitate the transformation of MMHg to DMHg via localized reduced thiol groups (Jonsson et al., 2016), with a proposed disproportionation reaction mechanism of two MMHg molecules to form DMHg and iHg. Inorganic Hg could be reduced to Hg^0 or be scavenged, while DMHg could evade to the atmosphere as previously highlighted. Complexation of MMHg to dissolved thiols in DOM could also reduce uptake of MMHg by phytoplankton (Lee and Fisher 2017) reducing MMHg bioavailability. MMHg-DOM complexes can also undergo enhanced photodemethylation (Qian et al., 2014) in surface waters, although the specific mechanisms remain debated (Barkay and Gu

2021). Additional Arctic seasonal studies are needed to characterize the types of DOM and its role in driving MeHg biogeochemical processes in the water column. Collectively though, our data and literature support biotically mediated MeHg demethylation during the development of the spring bloom.

Interestingly, deeper waters (100 to 500 m) also show a net loss of MeHg concentrations, with an average loss rate of 0.015 ± 0.011 d^{-1} (n = 7) in the 100 - 200 m depth interval. While potential phytoplankton demethylation could explain MeHg losses in surface waters, we expect different biotic processes to affect MeHg losses in subsurface and bottom waters. Recent research has demonstrated that the presence of the *merB* gene, found in certain bacteria and responsible for the demethylation of MeHg to Hg^{II}, is present in deep waters of the Arctic Ocean (Bowman et al., 2020). In bacteria, the *mer* operon, encoding for *merA* and *merB* genes, exists primarily as a detoxifying mechanism for high concentrations of Hg, in a process called reductive demethylation. Lineages of a particular bacterial strain genome containing *merA* and *merB*, with high resistance and strong degradation capacity of MeHg, are present in polar regions (Sanz-Sáez et al., 2022). On our transect, potential reductive demethylators (*Alteromonas*, *Marinobacter*, and *Oleibacter*) are present, but in low relative abundance during both sampling periods compared to the entire bacterial and archaeal community (SI Text). However, bottom waters at shelf stations had higher total abundances of bacteria and higher relative abundances of potential demethylators than surface waters in late winter and could support MeHg degradation during the winter-spring transition (SI Text). This includes methanotrophic bacteria and sulfate reducing bacteria, which can also participate in oxidative demethylation of MeHg under anoxic conditions (Barkay and Gu, 2021).

While dark abiotic demethylation could influence our losses of MeHg in deep waters, more research is needed to uncover these mechanisms. Dissolved CHOS compounds, seen in both surface and deeper waters in both late winter and spring (SI Fig. 6), could facilitate transformation and demethylation of MMHg as previously discussed. Additionally, resuspension of sediments may supply manganese oxide to bottom waters, resulting in both the demethylation and scavenging of MMHg and iHg (Vlassopolous et al., 2018, Murphy et al., 2021, Kohler et al., 2022a). However, due to the uncertainty of these potential abiotic processes, we hypothesize much of our MeHg in deeper waters is also biotically demethylated from late winter into spring.

3.7 Hg in basin deep waters (> 500 m)

Bottom waters below 500 m at stations P6 and P7 are elevated in THg compared to the shelf stations (SI Fig. 1). These elevated concentrations in EBDW could contain additional Hg from resuspended sediment or sinking particles, as suggested in the Canadian Basin (Agather et al., 2019). As these basin stations are close to the shelf break, turbidity along the continental slope caused by the West Spitsbergen Current may resuspend and deliver Hg-rich particles into the basin. Throughout the Arctic winter (December to March), overturning on the Barents Sea shelf generates a nepheloid layer of suspended sediment which can sink as dense water plumes into the basin (Rudels et al., 2004, Gardner et al., 2022, Rogge et al., 2022). High concentrations of Hg and other trace elements in surface sediments in the Eurasian Basin have suggested hydrodynamic transport and scavenging of particles sourced from the shelf (Kohler et al., 2022b). Beam transmittance data (SI Fig. 10), however does not support significant resuspension of sediments in basin waters. For MeHg, stations P6 and P7 show similar patterns in late winter and spring, with the highest MeHg concentrations observed at 500 m and below. In EBDW, MeHg concentrations remain elevated above 170 fmol L^{-1} at P7 until 2500 m depth. Compared to the shelf, EBDW and deeper waters remain enriched in MeHg. These observations are in line with previous measurements in the Fram Strait with maximum MeHg between 400 – 1000 m (Petrova et al., 2020). Diffusion of porewater-derived MeHg could help explain elevated MeHg concentrations along the continental slope by station P6 (Kim et al., 2020b). Although both MeHg and THg concentrations in the deep basin agree with previous literature (Wang et al., 2012, Heimbürger et al., 2015), our sampling with standard Niskin bottles lends a degree of caution.

3.8 Seasonal cycle of Hg in the northern Barents Sea

Our observations for both THg and MeHg suggest a distinct seasonality of Hg in the northern Barents Sea marginal ice zone from late winter to spring. Based on our analysis, we conclude that the main drivers of both THg and MeHg changes in surface waters are ultimately driven by seasonal Hg inputs and the biotically driven processes of the phytoplankton spring bloom. In deeper waters, biotic demethylation is likely to play a more important role than abiotic demethylation mechanisms. A previous study suggested iHg seasonality in this region during the transition from summer to winter, with no significant change in MeHg concentrations (Kohler et al., 2022a). By assuming Hg follows a distinct seasonal cycle in the Arctic Ocean every year, we combined our observations from late winter and spring 2021 with that of summer and early winter 2019 (Kohler et al., 2022c,d) to illustrate a simple seasonal cycle of Hg over the course of a year in the northern Barents Sea surface waters (Fig. 6). To best illustrate the seasonal dynamics of THg and MeHg, we integrated our results from the surface to 100 m depth for each station (Tables S4 & S5), where most biological productivity and Hg input occurs.

Seasonal Cycle of Hg in the Northern Barents Sea

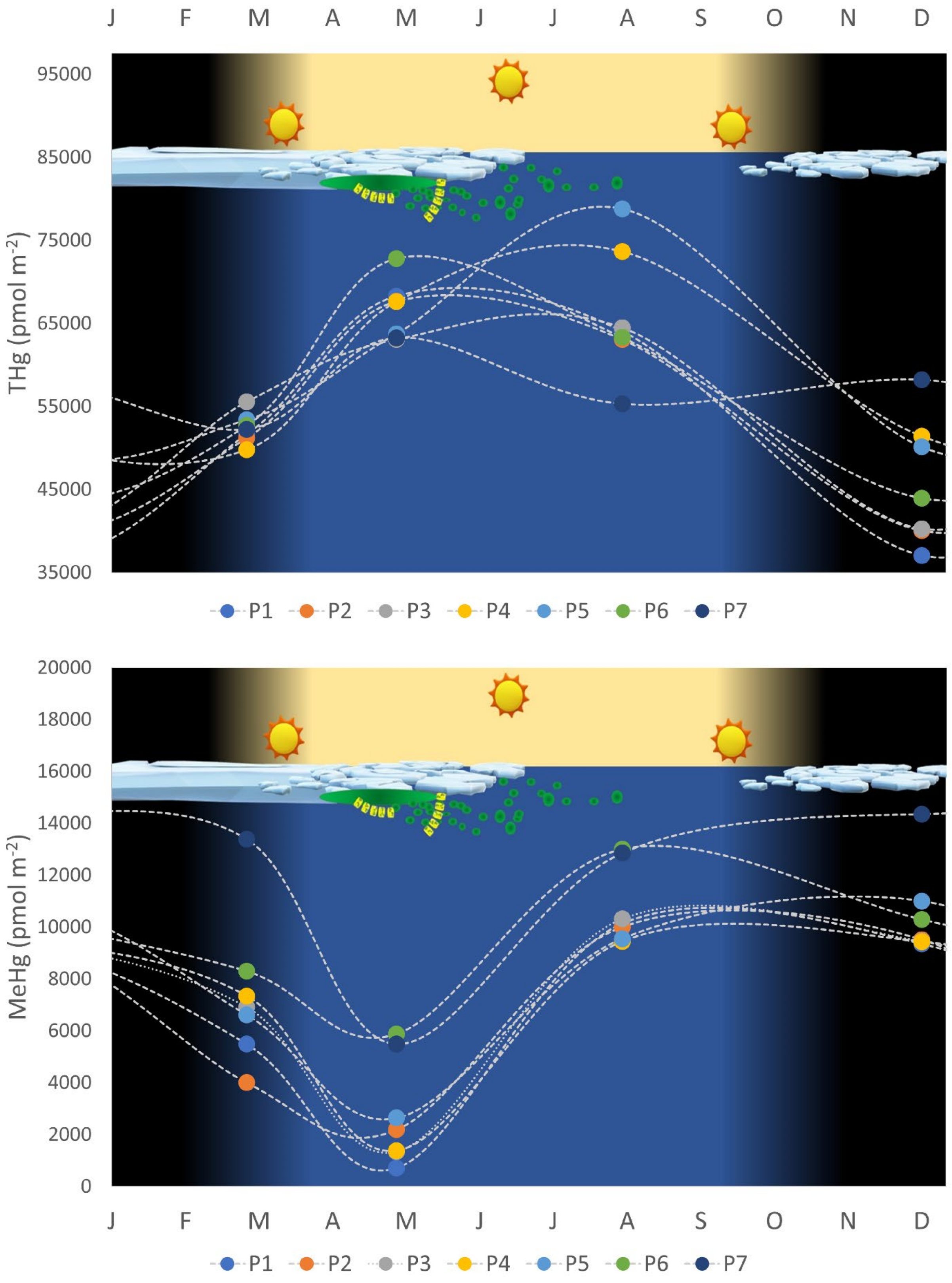

Figure 6: Integrated water column (0 to 100 m) observations of THg (top) and MeHg (bottom) from seasonal cruises (this study) and a previous study (Kohler et al., 2022a) in the northern Barents Sea. Graphs are superimposed on a simplified Arctic seasonal cycle in the marginal ice zone with polar day occurring between April and August and polar night beginning November until February. Green particles represent the development of the ice algal and phytoplankton spring blooms. Integrated pools for THg and MeHg are found in Tables S4 and S5. The x-axis is in months. Note the difference in scales on the y-axis.

Seasonal patterns of both THg and MeHg emerge and appear to be driven by the development of biological activity. The THg pools are higher during the polar day, while MeHg pools are at the minimum at the onset of the phytoplankton bloom and maximum in the second half of the year. As hypothesized, seasonal inputs and biological activity increase THg concentrations in surface waters. To better assess how relevant environmental drivers impact seasonal THg and MeHg concentrations, a PCA was conducted for each seasonal cruise (Fig. 7), with the first two principal components explaining > 60% of the variance for each cruise (Table S7). Clustering of THg with biological parameters POC and chlorophyll *a* in spring and summer suggest seasonal changes in THg concentrations are driven by biological activity and its partitioning to the particulate phase. Notably, this includes potential uptake of Hg species, transformation to MeHg during remineralization of POC, and downward transport with sinking particles. Sinking POC supports the production of subsurface in situ MeHg throughout polar day (Heimbürger et al., 2015), reflected in increasing MeHg pools progressing into summer (Fig. 6) and the general trend of positive MeHg loadings on the first component with depth, nutrients, and salinity for the spring and summer cruises. Late summer POC fluxes (Bodur et al., 2023), and increased proportions of manganese oxides leading into the polar night (Xiang and Lam 2020) lower THg pools by early winter (Kohler et al., 2022a).

Less clear is the behavior of both THg and MeHg throughout the polar night into late winter. It was proposed that potential scavenging by manganese oxides could be a driver of THg during Arctic winter (Kohler et al., 2022a), although a negative trend in THg pools from early winter to late winter is not observed (Fig. 6). We speculate that changes in Hg speciation, such as increased proportions of gaseous Hg^0 and DMHg could protect against scavenging losses. A recent experimental study argued that gross dark reduction rates of Hg^{II} to Hg^0 are significant in both photic and aphotic zones, with dark reduction most likely dominant in the Arctic except during polar day (Lamborg et al., 2021). Reduction could be driven by bacteria with the *merA* gene, and potentially include bacteria with both *merA* and *merB,* facilitating declining MeHg pools throughout the polar night (Fig. 6). The bacterial community in this region shifts from carbon cycling in summer to nitrogen cycling in winter (Thiele et al., 2023), suggesting a possible link between MeHg and the nitrogen cycle (Despins et al., 2023) during the polar night. In our PCA analysis, we observed that MeHg and nitrite (NO_2) exhibited opposite loadings on PC2 for all cruises (Fig. 7). This observation could link nitrite-oxidizing *Nitrospina,* known to harbor and express *hgcAB*-like proteins for Hg methylation (Gionfriddo et al., 2016, Villar et al., 2020), as a driver for in situ seasonal MeHg concentrations in the Arctic. Our in situ concentration data however, show a net loss of the MeHg pool from winter to late winter (Fig. 6). As our studies comprise two different sampling years (2019 vs. 2021), more seasonal and interannual studies are needed to fully understand the drivers of MeHg concentrations in the Arctic water column.

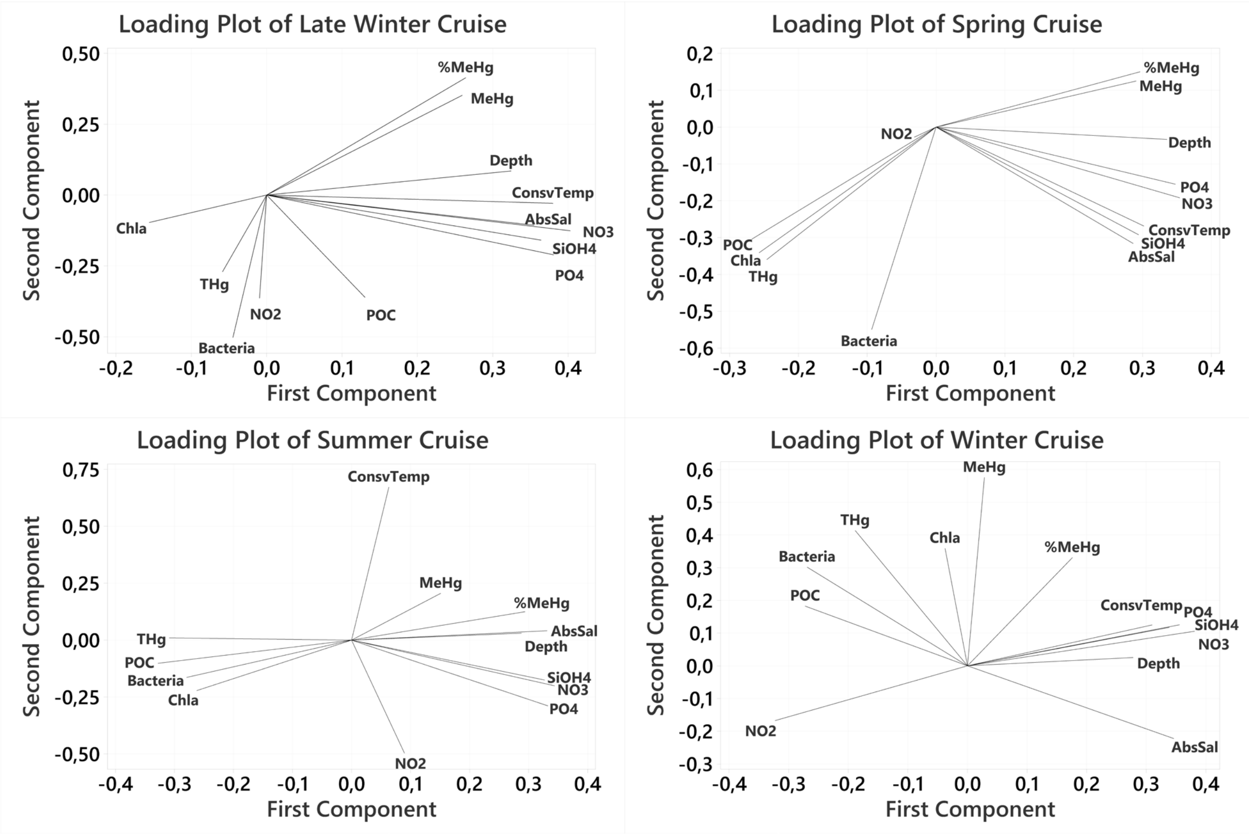

Figure 7: Principal component analysis (PCA) loadings plot for each seasonal cruise in the northern Barents Sea from this study and previous cruises where Hg observations are available (<

500 m only) (Kohler et al., 2022a). Rotation is orthogonal with the first two principal components plotted. Selected environmental parameters included depth, conservative temperature (ConsvTemp), absolute salinity (AbsSal), bacterial abundance (bacteria), chlorophyll *a* (Chla), particulate organic carbon (POC), nitrate (NO3), nitrite (NO2), phosphate (PO4), and silicate (SiOH4), THg, MeHg, and %MeHg.

To the best of our knowledge, only one model has attempted to represent seasonal cycling of Hg in the Arctic Ocean (Fisher et al., 2012). In this model, sources and sinks of Hg are categorized by month, with subsurface waters resupplying Hg to surface waters through vertical mixing. However, the latest Arctic budget highlights that export of Hg to deeper waters is most likely underestimated (Dastoor et al., 2022), further supporting our hypothesis that seasonal changes in Hg may be driven by spring Hg inputs and changes in the particulate phase. Our new seasonal data help fill in this knowledge gap but continue to remain a "seasonal snapshot" from both a seasonal and interannual perspective. Recent studies on seasonality in this region highlight large seasonal and interannual variability in the northern Barents Sea regarding water masses and sea ice dynamics (Jones et al., 2023, Kohlbach et al., 2023, Van Engeland et al., 2023). Specifically, interannual variability may exert a greater impact on perceived seasonality, as our four cruises were sampled in two different years (2019 vs. 2021). As a result, our interpretations between the spring to summer transition and the early winter to late winter transition are subject to both seasonal and interannual variability, and thus more speculation. Nevertheless, we propose that our seasonal cycle of Hg in the northern Barents Sea is supported by our observational data and is reflected in current literature on Arctic Hg cycling.

4 Conclusion

We show that both THg and MeHg concentrations in the water column of the northern Barents Sea exhibit dynamic changes throughout the year. Variations in THg and MeHg are driven by seasonal processes during the early spring, such as Hg input to surface waters and biological activity. Notably, we observed a significant decline in MeHg concentrations during the development of the phytoplankton spring bloom. We suggest biotic demethylation mediated by phytoplankton and bacteria as the main mechanism underlying our observations. This demethylation by phytoplankton and bacteria during the spring bloom may mitigate the bioaccumulation of Hg up the food web. Although it is difficult to completely disentangle these losses and transformations of MeHg, our data suggests that potential seasonal uptake of MeHg during the spring bloom represents an important entry point of Hg into the Arctic marine ecosystem.

Using our current data, we constructed a simplified seasonal Hg cycle in the northern Barents Sea marginal ice zone and conducted additional analysis to try and identify major environmental parameters driving both THg and MeHg concentrations. THg was clustered with chlorophyll *a* and POC in spring and summer, suggesting seasonal changes of THg are modulated by changes in primary productivity, particles, and food web processes. MeHg concentrations also exhibited a seasonal pattern, with potential uptake and demethylation during spring, followed by hypothesized in situ production throughout the summer. Our simple seasonal cycle also encompasses potential interannual variability, which may underestimate additional drivers of Hg concentrations such as sea ice coverage and changing water masses. In addition, the northern Barents Sea has limited riverine inputs, highly variable sea ice coverage and a unique water mass distribution compared to the other Arctic shelf seas. Thus, the applicability of our proposed seasonal cycle may have limited use in other Arctic regions, like the river-influenced Siberian shelf seas or less biologically productive Central Arctic Ocean. Nevertheless, our study represents an important first step in identifying Hg seasonal processes and drivers in Arctic waters, with additional seasonal environmental data from the Nansen Legacy project available for use in budgets and models. We suggest future Arctic Hg budgets and coupled ocean-atmosphere/earth system models include an element of seasonality.

The projected climate driven inputs of increasing amounts of Hg from melting glaciers and thawing permafrost to Arctic shelf seas during the onset of the productive season may facilitate greater uptake of MMHg in the marine food web (Chételat et al., 2022). As ongoing climate change continues to transform the Arctic region, more research is needed to elucidate how region-specific seasonal processes affect Hg distributions in the Arctic Ocean and the surrounding shelf seas. Specifically, we suggest more studies examining the connection between demethylation and biological uptake in the marginal ice zones as well as seasonal measurements of gaseous Hg species. We suspect that these transformation processes and rates that control MeHg distributions in the water column, and subsequently uptake in biota, follow a seasonal pattern.

CRediT authorship contribution statement

Stephen G. Kohler: Conceptualization, methodology, validation, formal analysis, investigation, writing - original draft, visualization, funding acquisition. **Lars-Eric Heimbürger-Boavida**: conceptualization, methodology, validation, investigation, writing - review and editing, visualization, supervision. **Philipp Assmy:** investigation, formal analysis, writing - review and editing, visualization. **Oliver Müller:** investigation, formal analysis, writing - review and editing, visualization. **Stefan Thiele:** investigation, formal analysis, writing - review and editing. **Maria G. Digernes:** Investigation, formal analysis, visualization. **Kuria Ndungu:** writing - review and editing, supervision. **Murat V. Ardelan**: Conceptualization, methodology, writing - review and editing, funding acquisition, supervision.

Acknowledgements

Funding for this study was provided by The Nansen Legacy project (RCN# 276730) and the Anders Jahres fond til vitenskapens fremme. The authors would like to thank the captain, crew members, cruise leaders, and fellow scientists onboard R/V *Kronprins Haakon* for cruises Q1 and Q2. Specifically, the authors would like to thank L. Kull and M. Adams for assistance in collecting mercury samples onboard and N. Torres-Rodriguez and A. Dufour for assistance in analysis. Additional thanks are to the sea ice coring teams and under ice water sampling teams for help in collecting ice samples. We also thank N. Sanchez and M. Petrova for their insightful comments on this manuscript. Lastly, we thank F. A. Cnossen for her artistic design of the graphical abstract.

References

Agather, A. M., Bowman, K. L., Lamborg, C. H. & Hammerschmidt, C. R. Distribution of mercury species in the Western Arctic Ocean (US GEOTRACES GN01). *Marine Chemistry* **216**, 103686, https://doi.org/10.1016/j.marchem.2019.103686 (2019).

Andersson, M. E., Sommar, J., Gårdfeldt, K. & Lindqvist, O. Enhanced concentrations of dissolved gaseous mercury in the surface waters of the Arctic Ocean. *Marine Chemistry* **110**, 190-194, https ://doi.org/10.1016/j.marchem.2008.04.002 (2008).

Araujo, B. F., Osterwalder, S., Szponar, N., Lee. D., Petrova, M. V., Pernov, J. B., Ahmed, S., Heimbürger-Boavida, L-E., Laffont, L., Teisserenc, R., Tananaev, N., Nordstrom, C., Magand, O., Stupple, G., Skov, H., Steffen, A., Bergquist, B., Pfaffhuber, K. A., Thomas, J. L., Scheper, S., Petäjä, T., Dommergue, A., & Sonke, J.E. Mercury isotope evidence for Arctic summertime re-emission of mercury from the cryosphere. *Nature Communications* **13**, 4956, https ://doi.org/10.1038/s41467-022-32440-8 (2022).

Ardyna, M., Babin, M., Gosselin, M., Devred, E., Rainville, L., & Tremblay, J-É. Recent Arctic Ocean sea ice loss triggers novel fall phytoplankton blooms. *Geophysical Research Letters* **41**, 6207-6212, https://doi.org/10.1002/2014GL061047 (2014).

Assmy, P., Fernández-Méndez, M., Duarte, P., Meyer, A., Randelhoff, A., Mundy, C. J., Olsen, L. M., Kauko, H. M., Bailey, A., Chierici, M., Cohen, L., Doulgeris, A. P., Ehn, J. K., Fransson, A., Gerland, S., Hop, H., Hudson, S. R., Hughes, N., Itkin, P., Johnsen, G., King, J. A., Koch, B. P., Koenig, Z., Kwasniewski, S., & Granskog, M. A. Leads in Arctic pack ice enable early phytoplankton blooms below snow-covered sea ice. *Scientific Reports* **7**, 40850, https://doi.org/10.1038/srep40850 (2017).

[dataset] Assmy, P., Gradinger, R., Edvardsen, B., Wold, A., Goraguer, L., & Wiktor, J. Phytoplankton biodiversity Nansen Legacy Q1 (Norwegian Polar Institute, 2022a) https://doi.org/10.21334/npolar.2022.e6521515

[dataset] Assmy, P., Gradinger, R., Edvardsen, B., Wold, A., Goraguer, L., Wiktor, J., Tatarek, A., & Smoła, Z. Phytoplankton biodiversity Nansen Legacy Q2 (Norwegian Polar Institute, 2022b) https://doi.org/10.21334/npolar.2022.9c05c643

Barkay, T. & Gu, B. Demethylation─the other side of the mercury methylation coin: a critical review. *ACS Environmental Au* **2**, 77-97, https ://doi.org/10.1021/acsenvironau.1c00022 (2021).

Basu, N., Abass, K., Dietz, R., Krümmel, E., Rautio, A., & Weihe, P. The impact of mercury contamination on human health in the Arctic: A state of the science review. *Science of the Total Environment* **831**, 154793, https://doi.org/10.1016/j.scitotenv.2022.154793 (2022).

Baya, P. A., Gosselin, M., Lehnherr, I., St Louis, V. L. & Hintelmann, H. Determination of monomethylmercury and dimethylmercury in the Arctic marine boundary layer. *Environmental Science & Technology* **49**, 223-232, https ://doi.org/10.1021/es502601z (2015).

Beattie, S. A., Armstrong, D., Chaulk, A., Comte, J., Gosselin, M., & Wang, F. Total and methylated mercury in Arctic multiyear sea ice. *Environmental Science & Technology* **48**, 5575-5582, https://doi.org/10.1021/es5008033 (2014).

Black, F. J., Conaway, C. H. & Flegal, A. R. Stability of dimethyl mercury in seawater and its conversion to monomethyl mercury. *Environmental Science & Technology* **43**, 4056-4062, https ://doi.org/10.1021/es9001218 (2009).

Bodur, Y. V., Renaud, P. E., Goraguer, L., Amargant-Arumí, M., Assmy, P., Dąbrowska, A., Marquardt, M., Renner, A. H. H., Tatarek, A., & Reigstad, M. Seasonal patterns of vertical flux in the northwestern Barents Sea under Atlantic Water influence and sea-ice decline. *Progress in Oceanography*, **219**, 103132, https://doi.org/10.1016/j.pocean.2023.103132 (2023).

Bowman, K. L., Collins, R. E., Agather, A. M., Lamborg, C. H., Hammerschmidt, C. R., Kaul, D., Dupont, C. L., Christensen, G. A., & Elias, D. A. Distribution of mercury-cycling genes in the Arctic and equatorial Pacific Oceans and their relationship to mercury speciation. *Limnology and Oceanography* **65**, S310-S320, https://doi.org/10.1002/lno.11310 (2020).

Bravo, A. G., Le Faucheur, S., Monperrus, M., Amouroux, D. & Slaveykova, V. I. Species-specific isotope tracers to study the accumulation and biotransformation of mixtures of inorganic and methyl mercury by the microalga *Chlamydomonas reinhardtii*. *Environmental Pollution* **192**, 212-215, https://doi.org/10.1016/j.envpol.2014.05.013 (2014).

Burt, A., Wang, F., Pućko, M., Mundy, C-J., Gosselin, M., Philippe, B., Poulin, M., Tremblay, J-É., & Stern, G. A. Mercury uptake within an ice algal community during the spring bloom in first-year Arctic sea ice. *Journal of Geophysical Research : Oceans* **118**, 4746-4754, https://doi.org/10.1002/jgrc.20380 (2013).

Charette, M. A., Kipp, L. E., Jensen, L. T., Dabrowski, J. S., Whitmore, L. M., Fitzsimmons, J. N., Williford, T., Ulfsbo, A., Jones, E., Bundy, R. M., Vivancos, S. M., Pahnke, K., John, S. G., Xiang, Y., Hatta, M., Petrova, M. V., Heimbürger-Boavida, L-E., Bauch, D., Newton, R., Pasqualini, A., Agather, A. M., Amon, R. M. W., Anderson, R. F., Andersson, P. S., Benner, R., Bowman, K. L., Edwards, R. L., Gdaniec, S., Gerringa, L. J. A., González, A. G., Granskog, M., Haley, B., Hammerschmidt, C. R., Hansell, D. A., Henderson, P. B., Kadko, D. C., Kaiser, K., Laan, P., Lam, P. J., Lamborg, C. H., Levier, M., Li, X., Margolin, A. R., Measures, C., Middag, R., Millero, F. J., Moore, W. S., Paffrath, R., Planquette, H., Rabe, B., Reader, H., Rember, R., Rijkenberg, M. J. A., Roy-Barman, M., van der Loeff, M. R., Saito, M., Schauer, U., Schlosser, P., Sherrell, R. M., Shiller, A. M., Slagter, H., Sonke, J. E., Stedmon, C., Woosley, R. J., Valk, O., van Ooijen, J., & Zhang, R. The transpolar drift as a source of riverine and shelf-derived trace elements to the central Arctic Ocean. *Journal of Geophysical Research: Oceans* **125**, e2019JC015920, https://doi.org/10.1029/2019JC015920 (2020).

Chaulk, A., Stern, G. A., Armstrong, D., Barber, D. G. & Wang, F. Mercury distribution and transport across the ocean-sea-ice-atmosphere interface in the Arctic Ocean. *Environmental Science & Technology* **45**, 1866-1872, https://doi.org/10.1021/es103434c (2011).

Chételat, J., McKinney, M. A., Amyot, M., Dastoor, A., Douglas, T. A., Heimbürger-Boavida, L-E., Kirk, J., Kahilainen, K. K., Outridge, P. M., Pelletier, N., Skov, H., St. Pierre, K., Vuorenmaa, J., & Wang, F. Climate change and mercury in the Arctic: abiotic interactions. *Science of the Total Environment* **824**, 153715, https://doi.org/10.1016/j.scitotenv.2022.153715 (2022).

[dataset] Chierici, M., Jones, E., & Lødemel, H. H. Water column data on dissolved inorganic nutrients (nitrite, nitrate, phosphate and silicic acid) from the Nansen LEGACY joint cruise KH 2019706 with R.V. Kronprins Haakon, 5-27 August 2019 (Norwegian Marine Data Centre, 2021a) https://doi.org/10.21335/NMDC-1472517325

[dataset] Chierici, M., Jones, E., & Lødemel, H. H. Water column data on dissolved inorganic nutrients (nitrite, nitrate, phosphate and silicic acid) from the Nansen LEGACY seasonal cruise Q4, 2019711 with R.V. Kronprins Haakon (Norwegian Marine Data Centre, 2021b) https://doi.org/10.21335/NMDC-1629206101

Cossart, T., Garcia-Calleja, J., Worms, I. A. M., Tessier, E., Kavanagh, K., Pedrero, Z,. Amouroux, D., & Slaveykova, V. I. Species-specific isotope tracking of mercury uptake and transformations by pico-nanoplankton in an eutrophic lake. *Environmental Pollution* **288**, 117771, https://doi.org/10.1016/j.envpol.2021.117771 (2021).

Cossart, T., Garcia-Calleja, J., Santos, J. P., Kalahroodi, E. L., Worms, I. A. M., Pedrero, Z., Amouroux, D., & Slaveykova, V. I. Role of phytoplankton in aquatic mercury speciation and transformations. *Environmental Chemistry* **19**, 104-115, https://doi.org/10.1071/En22045 (2022).

Cutter, G. A., Casciotti, K., Croot, P., Geibert, W., Heimbürger, L-E., Lohan, M., Planquette, H., & van de Flierdt, T. Sampling and sample-handling protocols for GEOTRACES Cruises, Version 3.0. http://dx.doi.org/10.25607/OBP-2 (2017)

Dastoor, A., Angot, H., Bieser, J., Christensen, J. H., Douglas, T. A., Heimbürger-Boavida, L-E., Jiskra, M., Mason, R. P., McLagan, D. S., Obrist, D., Outridge, P. M., Petrova, M. V., Ryjkov, A., St. Pierre, K. A., Schartup, A. T., Soerensen, A. L., Toyota, K., Travnikov, O., Wilson, S. J., & Zdanowicz, C. Arctic mercury cycling. *Nature Reviews Earth & Environment*, https://doi.org/10.1038/s43017-022-00269-w (2022).

Despins, M. C., Mason, R. P., Aguilar-Islas, A. M., Lamborg, C. H., Hammerschmidt, C. R., & Newell, S. E. Linked mercury methylation and nitrification across oxic subpolar regions. *Frontiers in Environmental Chemistry* **4**, 1109537, https://doi.org/10.3389/fenvc.2023.1109537 (2023).

Dietz, R., Letcher, R. J., Aars, J., Andersen, M., Boltunov, A., Born, E. W., Ciesielski, T. M., Das, K., Dastnai, S., Derocher, A. E., Desforges, J-P., Eulaers, I., Ferguson, S., Hallanger, I. G., Heide-Jørgensen, M. P., Heimbürger-Boavida, L-E., Hoekstra, P. F., Jenssen, B. M., Kohler, S. G., Larsen, M. M., Lindstrøm, U., Lippold, A., Morris, A., Nabe-Nielsen, J., Nielsen, N. H., Peacock, E., Pinzone, M., Rigét, F. F., Rosing-Asvid, A., Routti, H., Siebert, U., Stenson, G., Stern, G., Strand, J., Søndergaard, J., Treu, G., Víkingsson, G. A., Wang, F., Welker, J. M., Wiig, Ø., Wilson, S. J., & Sonne, C. A risk assessment review of mercury exposure in Arctic marine and terrestrial mammals. *Science of the Total Environment* **829**, 154445, https://doi.org/10.1016/j.scitotenv.2022.154445 (2022).

DiMento, B. P., Mason, R. P., Brooks, S. & Moore, C. The impact of sea ice on the air-sea exchange of mercury in the Arctic Ocean. *Deep Sea Research Part I* **144**, 28-38, https://doi.org/10.1016/j.dsr.2018.12.001 (2019).

Dommergue, A., Larose, C., Faïn, X., Clarisse, O., Foucher, D., Hintelmann, H., Schneider, D., & Ferrari, C. P. Deposition of mercury species in the Ny-Alesund area (79 degrees N) and their transfer during snowmelt. *Environmental Science & Technology* **44**, 901-907, https://doi.org/10.1021/es902579m (2010).

Durnford, D. & Dastoor, A. The behavior of mercury in the cryosphere: A review of what we know from observations. *Journal of Geophysical Research: Atmospheres* **116**, https://doi.org/10.1029/2010jd014809 (2011).

Dybwad, C., Lalande, C., Bodur, Y. V., Henley, S. F., Cottier, F., Ershova, E. A., Hobbs, L., Last, K. S., Dąbrowska, A. M., & Reigstad, M. The influence of sea ice cover and Atlantic Water advection on annual particle export north of Svalbard. *Journal of Geophysical Research: Oceans* **127**, e2022JC018897, https://doi.org/10.1029/2022jc018897 (2022).

Fisher, J. A., Jacob, D. J., Soerensen, A. L., Amos, H. M., Steffen, A., & Sunderland, E. M. Riverine source of Arctic Ocean mercury inferred from atmospheric observations. *Nature Geoscience* **5**, 499-504, https://doi.org/10.1038/ngeo1478 (2012).

Gardner, W. D., Richardson, M. J., Mishonov, A. V., Lam, P. J. & Xiang, Y. Distribution, sources, and dynamics of particulate matter along Trans-Arctic sections. *Journal of Geophysical Research: Oceans* **127**, e2021JC017970, doi:ARTN https://doi.org/10.1029/2021JC017970 (2022).

[dataset] Gerland, S. CTD data from Nansen Legacy Cruise - Seasonal Cruise Q1 (Norwegian Marine Data Centre, 2022) https://doi.org/10.21335/NMDC-1491279668

Gionfriddo, C. M., Tate, M. T., Wick, R. R., Schultz, M. B., Zemla, A., Thelen, M. P., Schofield, R., Krabbenhoft, D. P., Holt, K. E., & Moreau, J. W. Microbial mercury methylation in Antarctic sea ice. *Nature Microbiology* **1**, 16127, https://doi.org/10.1038/nmicrobiol.2016.127 (2016)

Heimbürger, L-E., Sonke, J. E., Cossa, D., Point, D., Lagane, C., Laffont, L., Galfond, B. T., Nicolaus, M., Rabe, B., & van der Loeff, M. R. Shallow methylmercury production in the marginal sea ice zone of the central Arctic Ocean. *Scientific Reports* **5**, 10318, https://doi.org/10.1038/srep10318 (2015).

Huang, S., Wang, F., Yuan, T., Song, Z., Wu, P., & Zhang, Y. Modeling the mercury cycle in the sea ice environment: a buffer between the polar atmosphere and ocean. *Environmental Science & Technology* **57**, 14589-14601, https://doi.org/10.1021/acs.est.3c05080 (2023).

[dataset] Jones, E., Chierici, M., Lødemel, H. H., Møgster, J., & Fonnes, L. L. Water column data on dissolved inorganic nutrients (nitrite, nitrate, phosphate and silicic acid) from Process (P) stations during the Nansen LEGACY seasonal cruise Q1, 2021703, with R.V.

Kronprins Haakon, 4-17 March 2021 (Norwegian Marine Data Centre, 2022a) https://doi.org/10.21335/NMDC-762320451

[dataset] Jones, E., Chierici, M., Lødemel, H. H., Møgster, J., & Fonnes, L. L. Water column data on dissolved inorganic nutrients (nitrite, nitrate, phosphate and silicic acid) from Process (P) stations during the Nansen LEGACY seasonal cruise Q2, 2021704, with R.V. Kronprins Haakon, 30 April - 18 May 2021 (Norwegian Marine Data Centre, 2022b) https://doi.org/10.21335/NMDC-487023368

Jones, E. M., Chierici, M., Fransson, A., Assmann, K. M., Renner, A. H. H., & Lødemel, H. H. Inorganic carbon and nutrient dynamics in the marginal ice zone of the Barents Sea: seasonality and implications for ocean acidification. *Progress in Oceanography*, 103131, https://doi.org/10.1016/j.pocean.2023.103131 (2023).

Jonsson, S., Mazrui, N. M. & Mason, R. P. Dimethylmercury formation mediated by inorganic and organic reduced sulfur surfaces. *Scientific Reports* **6**, 27958, https://doi.org/10.1038/srep27958 (2016).

Jonsson, S., Nerentorp Mastromonaco, M., Wang, F., Bravo, A. G., Cairns, W. R. L., Chételat, J., Douglas, T. A., Lescord, G., Ukonmaanaho, L., & Heimbürger-Boavida, L-E. Arctic methylmercury cycling. *Science of the Total Environment* **850**, 157445, https://doi.org/10.1016/j.scitotenv.2022.157445 (2022a).

Jonsson, S., Nerentorp Mastromonaco, M. G., Gårdfeldt, K. & Mason, R. P. Distribution of total mercury and methylated mercury species in Central Arctic Ocean water and ice. *Marine Chemistry* **242**, 104105, https://doi.org/10.1016/j.marchem.2022.104105 (2022b).

Kim, H., Kwon, S. Y., Lee, K., Lim, D., Han, S., Kim, T-W., Joo, Y. J., Lim, J., Kang, M-H., & Nam, S-I. Input of terrestrial organic matter linked to deglaciation increased mercury transport to the Svalbard fjords. *Scientific Reports* **10**, 3446, https://doi.org/10.1038/s41598-020-60261-6 (2020a).

Kim, J., Soerensen, A. L., Kim, M. S., Eom, S., Rhee, T. S., Jin, Y. K., & Han, S. Mass budget of methylmercury in the East Siberian Sea: The Importance of Sediment Sources. *Environmental Science & Technology* **54**, 9949-9957, https://doi.org/10.1021/acs.est.0c00154 (2020b).

Kohlbach, D., Goraguer, L., Bodur, Y. V., Müller, O., Amargant-Arumí, M., Blix, K., Bratbak, G., Chierici, M., Dąbrowska, A. M., Dietrich, U., Edvardsen, B., García, L. M., Gradinger, R., Hop, H., Jones, E., Lundesgaard, Ø., Olsen, L. M., Reigstad, M., Saubrekka, K., Tatarek, A., & Assmy, P. Earlier sea-ice melt extends the oligotrophic summer period in the Barents Sea with low algal biomass and associated low vertical flux. *Progress in Oceanography* **213**, 103018, https://doi.org/10.1016/j.pocean.2023.103018, (2023).

Kohler, S. G. Heimbürger-Boavida, L-E., Petrova, M. V., Digernes, M. G., Sanchez, N., Dufour, A., Simić, A., Ndungu, K., & Ardelan, M. V. Arctic Ocean's wintertime mercury concentrations limited by seasonal loss on the shelf. *Nature Geoscience* **15**, 621-626, https://doi.org/10.1038/s41561-022-00986-3 (2022a).

Kohler, S. G., Kull L. M., Heimbürger-Boavida, L-E., Ricardo de Freitas, T., Sanchez, N., Ndungu, K., & Ardelan, M. V. Distribution pattern of mercury in northern Barents Sea and Eurasian Basin surface sediment. *Marine Pollution Bulletin* **185**, 114272, https://doi.org/10.1016/j.marpolbul.2022.114272 (2022b).

[dataset] Kohler, S. G. Heimbürger-Boavida, L-E., Petrova, M. V., Digernes, M. G., Sanchez, N., Dufour, A., Simić, A., Ndungu, K., & Ardelan, M. V. Concentrations of total mercury, total methylated mercury, and selected trace elements in the northern Barents Sea as part of the Nansen Legacy project, Cruise 2019706 Q3 (Norwegian Marine Data Centre, 2022c); https://doi.org/10.21335/NMDC-416151559

[dataset] Kohler, S. G. Heimbürger-Boavida, L-E., Petrova, M. V., Digernes, M. G., Sanchez, N., Dufour, A., Simić, A., Ndungu, K., & Ardelan, M. V. Concentrations of total mercury, total methylated mercury, and selected trace elements in the northern Barents Sea as part of the Nansen Legacy project, Cruise 2019711 Q4 (Norwegian Marine Data Centre, 2022d); https://doi.org/10.21335/NMDC-1871554897

Lamborg, C. H., Hansel, C. M., Bowman, K. L., Voelker, B. M., Marsico, R. M., Oldham, V. E., Swarr, G. J., Zhang, T., & Ganguli, P. M. (2021). Dark reduction drives evasion of mercury from the ocean. *Frontiers in Environmental Chemistry*, ***2***, 659085, https://doi.org/10.3389/fenvc.2021.659085 (2021).

Lee, C. S. & Fisher, N. S. Methylmercury uptake by diverse marine phytoplankton. *Limnology and Oceanography* **61**, 1626-1639, https://doi.org/10.1002/lno.10318 (2016)

Lee, C. S. & Fisher, N. S. Bioaccumulation of methylmercury in a marine diatom and the influence of dissolved organic matter. *Marine Chemistry* **197**, 70-79, https://doi.org/10.1016/j.marchem.2017.09.005 (2017).

Lehnherr, I., St Louis, V. L., Hintelmann, H. & Kirk, J. L. Methylation of inorganic mercury in polar marine waters. *Nature Geoscience* **4**, 298-302, https://doi.org/10.1038/Ngeo1134 (2011).

Li, Y., Li, D., Song, B. & Li, Y. The potential of mercury methylation and demethylation by 15 species of marine microalgae. *Water Research* **215**, 118266, https://doi.org/10.1016/j.watres.2022.118266 (2022).

Liang, X., Zhong, H., Johs, A., Lei, P., Zhang, J., Taş, N., Zhang, L., Zhao, L., Zhu, N., Yin, X., Wang, L., Zeng, E. Y., Gao, Y., Zhao, J., Pelletier, D. A., Pierce, E. M., & Gu, B. Light-independent phytoplankton degradation and detoxification of methylmercury in water. *Nature Water* **1**, 705-715, https://doi.org/10.1038/s44221-023-00117-1 (2023).

Loeng, H. Features of the physical oceanographic conditions of the Barents Sea. *Polar Research* **10**, 5-18, https://doi.org/10.3402/polar.v10i1.6723 (1991).

Lundesgaard, Ø., Sundfjord, A., Lind, S., Nilsen, F. & Renner, A. H. H. Import of Atlantic Water and sea ice controls the ocean environment in the northern Barents Sea. *Ocean Science* **18**, 1389-1418, https://doi.org/10.5194/os-18-1389-2022 (2022).

[dataset] Ludvigsen, M. CTD data from Nansen Legacy Cruise - Seasonal Cruise Q2 (Norwegian Marine Data Centre, 2022) https://doi.org/10.21335/NMDC-515075317

Luengen, A. C. & Flegal, A. R. Role of phytoplankton in mercury cycling in the San Francisco Bay estuary. *Limnology and Oceanography* **54**, 23-40, https://doi.org/10.4319/lo.2009.54.1.0023 (2009).

Marquardt, M., Goraguer, L., Assmy, P., Bluhm, B. A., Aaboe, S., Down, E., Patrohay, E., Edvardsen, B., Tatarek, A., Smoła, Z., Wiktor, J., & Gradinger, R. Seasonal dynamics of sea-ice protist and meiofauna in the northwestern Barents Sea. *Progress in Oceanography* **218**, 103128, https://doi.org/10.1016/j.pocean.2023.103128 (2023).

[dataset] Marquardt, M., Bodur, Y. V., Dubourg, P., & Reigstad, M. Concentration of particulate organic carbon (POC) and particulate organic nitrogen (PON) from the sea water and sea ice in the northern Barents Sea as part of the Nansen Legacy project, Cruise 2021703 Q1. (Norstore, 2022a) https://doi.org/10.11.582/2022.00053

[dataset] Marquardt, M., Bodur, Y. V., Dubourg, P., & Reigstad, M. Concentration of particulate organic carbon (POC) and particulate organic nitrogen (PON) from the sea water and

sea ice in the northern Barents Sea as part of the Nansen Legacy project, Cruise 2021704 Q2. (Norstore, 2022b) https://doi.org/10.11.582/2022.00054

[dataset] Marquardt, M., Bodur, Y. V., Dubourg, P., & Reigstad, M. Concentration of particulate organic carbon (POC) and particulate organic nitrogen (PON) from the sea water and sea ice in the northern Barents Sea as part of the Nansen Legacy project, Cruise 2019706 Q3. (Norstore, 2022c) https://doi.org/10.11.582/2022.00055

[dataset] Marquardt, M., Bodur, Y. V., Dubourg, P., & Reigstad, M. Concentration of particulate organic carbon (POC) and particulate organic nitrogen (PON) from the sea water and sea ice in the northern Barents Sea as part of the Nansen Legacy project, Cruise 2019711 Q4. (Norstore, 2022d) https://doi.org/10.11.582/2022.00048

Mason, R. P., Reinfelder, J. R. & Morel, F. M. M. Uptake, toxicity, and trophic transfer of mercury in a coastal diatom. *Environmental Science & Technology* **30**, 1835-1845, https://doi.org/10.1021/es950373d (1996).

Moore, C. W., Obrist, D., Steffen, A., Staebler, R. M., Douglas, T. A., Richter, A., & Nghiem, S. V. Convective forcing of mercury and ozone in the Arctic boundary layer induced by leads in sea ice. *Nature* 506, 81-84, https://doi.org/10.1038/nature12924 (2014).

Monperrus, M., Tessier, E., Amouroux, D., Leynaert, A., Huonnic, P., & Donard, O. F. X. Mercury methylation, demethylation and reduction rates in coastal and marine surface waters of the Mediterranean Sea. *Marine Chemistry* **107**, 49-63, https://doi.org/10.1016/j.marchem.2007.01.018 (2007).

Morelli, E., Ferrara, R., Bellini, B., Dini, F., Di Giuseppe, G., & Fantozzi, L. Changes in the non-protein thiol pool and production of dissolved gaseous mercury in the marine diatom *Thalassiosira weissflogii* under mercury exposure. *Science of the Total Environment* **408**, 286-293, https://doi.org/10.1016/j.scitotenv.2009.09.047 (2009).

[dataset] Müller, O., Petelenz, E., Tsagkaraki, T., Langvad, M., Grytaas, A., & Bratbak, G. Flow cytometry measurements (abundance of virus, bacteria and small protists (primarily <20µm)) during Nansen Legacy cruise 2021703 (from March 2nd to 24th in 2021) in the Northern Barents Sea (2023a) https://doi.org/10.21335/NMDC-282686035

[dataset] Müller, O., Petelenz, E., Tsagkaraki, T., Langvad, M., Thiele, S., Olsen, L., & Bratbak, G. Flow cytometry measurements (abundance of virus, bacteria and small protists (primarily <20µm)) during Nansen Legacy cruise 2021704 (from April 27th to May 20th in 2021)

in the Northern Barents Sea (2023b) https://doi.org/10.21335/NMDC-277392634

[dataset] Müller, O., Petelenz, E., Tsagkaraki, T., Langvad, M., Olsen, L., & Bratbak, G. Flow cytometry measurements (abundance of virus, bacteria and small protists (primarily <20µm)) during Nansen Legacy cruise 2019706 (from August 5th to 27th in 2019) in the Northern Barents Sea (2023c) https://doi.org/10.21335/NMDC-39569968

[dataset] Müller, O., Petelenz, E., Tsagkaraki, T., Langvad, M., Stabell, H., & Bratbak, G. Flow cytometry measurements (abundance of virus, bacteria and small protists (primarily <20µm)) during Nansen Legacy cruise 2019711 (from November 28th to December 17th in 2019) in the Northern Barents Sea (2023d) https://doi.org/10.21335/NMDC-2099951995

Murphy, S. A., Schwartz, G. E. & Brooks, S. C. Demethylation or Sorption? The fate of methylmercury in the presence of manganese dioxide. *Environmental Engineering Science* **38**, 224-230, https://doi.org/10.1089/ees.2020.0068 (2021).

Nerentorp Mastromonaco, M. G., Gårdfeldt, K., Langer, S. & Dommergue, A. Seasonal study of mercury species in the Antarctic sea ice environment. *Environmental Science & Technology* **50**, 12705-12712, https://doi.org/10.1021/acs.est.6b02700 (2016).

Nerentorp Mastromonaco, M. G., Gårdfeldt, K., Assmann, K. M., Langer, S., Delali, T., Shlyapnikov, Y. M., Zivkovic, I., & Horvat, M. Speciation of mercury in the waters of the Weddell, Amundsen and Ross Seas (Southern Ocean). *Marine Chemistry* **193**, 20-33, https://doi.org/10.1016/j.marchem.2017.03.001 (2017).

Pérez-Hernández, M. D., Pickart, R. S., Torres, D. J., Bahr, F., Sundfjord, A., Ingvaldsen, R., Renner, A. H. H., Beszczynska-Möller, A., von Appen, W-J., & Pavlov, V. Structure, transport, and seasonality of the Atlantic Water boundary current north of Svalbard: Results from a yearlong mooring array. *Journal of Geophyical Research : Oceans* **124**, 1679-1698, https://doi.org/10.1029/2018jc014759 (2019).

Petrova, M. V., Krisch, S., Lodeiro, P., Valk, O., Dufour, A., Rijkenberg, M. J. A., Achterberg, E. P., Rabe, B., van der Loeff, M. R., Hamelin, B., Sonke, J. E., Garnier, C., & Heimbürger-Boavida, L-E. Mercury species export from the Arctic to the Atlantic Ocean. *Marine Chemistry* **225**, 103855, https://doi.org/10.1016/j.marchem.2020.103855 (2020).

Point, D., Sonke, J. E., Day, R. D., Roseneau, D. G., Hobson, K. A., Vander Pol, S. S., Moors, A. J., Pugh, R. S., Donard, O. F. X., & Becker, P. R. Methylmercury photodegradation influenced by sea-ice cover in Arctic marine ecosystems. *Nature Geoscience* **4**, 188-194, https://doi.org/10.1038/Ngeo1049 (2011).

Pućko, M., Burt, A., Walkusz, W., Wang, F., Macdonald, R. W., Rysgaard, S., Barber, D. G., Tremblay, J-É., & Stern, G. A. Transformation of mercury at the bottom of the Arctic food web: an overlooked puzzle in the mercury exposure narrative. *Environmental Science & Technology* **48**, 7280-7288, https://doi.org/10.1021/es404851b (2014).

Qian, Y., Yin, X., Lin, H., Rao, B., Brooks, S. C., Liang, L., & Gu, B. Why dissolved organic matter enhances photodegradation of methylmercury. *Environmental Science & Technology Letters* **1**, 426-431, https://doi.org/10.1021/ez500254z (2014).

Ravichandran, M. Interactions between mercury and dissolved organic matter--a review. *Chemosphere* **55**, 319-331, https://doi.org/10.1016/j.chemosphere.2003.11.011 (2004).

[dataset] Reigstad, M. CTD Data from Nansen Legacy Cruise—Seasonal Cruise Q3 (Norwegian Marine Data Centre, 2022); https://doi.org/10.21335/NMDC-1107597377

Reigstad, M., Wassmann, P., Wexels Riser, C., Øygarden, S. & Rey, F. Variations in hydrography, nutrients and chlorophyll a in the marginal ice-zone and the central Barents Sea. *Journal of Marine Systems* **38**, 9-29, https://doi.org/10.1016/S0924-7963(02)00167-7 (2002).

Rogge, A., Janout, M., Loginova, N., Trudnowska, E., Hörstmann, C., Wekerle, C., Oziel, L., Schourup-Kristensen, V., Ruiz-Castillo, E., Schulz, K., Povazhnyy, V. V., Iversen, M. H., & Waite, A. M. Carbon dioxide sink in the Arctic Ocean from cross-shelf transport of dense Barents Sea water. *Nature Geoscience* **16**, 82-88, https://doi.org/10.1038/s41561-022-01109-8 (2022).

Rudels, B., Muench, R. D., Gunn, J., Schauer, U. & Friedrich, H. J. Evolution of the Arctic Ocean boundary current north of the Siberian shelves. *Journal of Marine Systems* **25**, 77-99, https://doi.org/10.1016/S0924-7963(00)00009-9 (2000).

Rudels, B., Jones, E. P., Schauer, U. & Eriksson, P. Atlantic sources of the Arctic Ocean surface and halocline waters. *Polar Research* **23**, 181-208, https://doi.org/10.1111/j.1751-8369.2004.tb00007.x (2004).

Sanz-Sáez, I., Pereira-García, C., Bravo, A. G., Trujillo, L., Pla i Ferriol, M., Capilla, M., Sánchez, P., Martín-Doimeadios, R. C. R., Acinas, S. G., & Sánchez, O. Prevalence of heterotrophic methylmercury detoxifying bacteria across oceanic regions. *Environmental Science & Technology* **56**, 3452-3461, https://doi.org/10.1021/acs.est.1c05635 (2022).

Schartup, A. T., Soerensen, A. L. & Heimbürger-Boavida, L-E. Influence of the Arctic Sea-Ice regime shift on sea-ice methylated mercury trends. *Environmental Science & Technology Letters* **7**, 708-713, https://doi.org/10.1021/acs.estlett.0c00465 (2020).

Schlitzer, R., 2021. Ocean Data View, odv.awi.de.

Schroeder, W. H., Anlauf, K. G., Barrie, L. A., Lu, J. Y., Steffen, A., Schneeberger, D. R., & Berg, T. Arctic springtime depletion of mercury. *Nature* **394**, 331-332, https://doi.org/10.1038/28530 (1998).

Sellers, P., Kelly, C. A., Rudd, J. W. M. & MacHutchon, A. R. Photodegradation of methylmercury in lakes. *Nature* **380**, 694-697, https://doi.org/10.1038/380694a0 (1996).

Soerensen, A. L., Jacob, D. J., Schartup, A. T., Fisher, J. A., Lehnherr, I., St. Louis, V. L., Heimbürger, L-E., Sonke, J. E., Krabbenhoft, D. P., & Sunderland, E. M. A mass budget for mercury and methylmercury in the Arctic Ocean. *Global Biogeochemical Cycles* **30**, 560–575, https://doi.org/10.1002/2015GB005280 (2016).

Sonke, J. E., Teisserenc, R., Heimbürger-Boavida, L-E., Petrova, M. V., Marusczak, N., Le Dantec, T., Chupakov, A. V., Li, C., Thackray, C. P., Sunderland, E. M., Tananaev, N., & Pokrovsky, O. S. Eurasian river spring flood observations support net Arctic Ocean mercury export to the atmosphere and Atlantic Ocean. *Proceedings of the National Academy of Sciences USA* **115**, E11586-E11594, https://doi.org/10.1073/pnas.1811957115 (2018).

[dataset] Steer, A., & Divine, D. Sea ice concentrations in the northern Barents Sea and the area north of Svalbard at Nansen Legacy stations during 2017-2021. (Norwegian Polar Institute, 2023) https://doi.org/10.21334/npolar.2023.24f2939c

Strass, V. H. & Nöthig, E. M. Seasonal shifts in ice edge phytoplankton blooms in the Barents Sea related to the water column stability. *Polar Biology* **16**, 409-422, https://doi.org/10.1007/BF02390423 (1996).

Sundfjord, A., Assmann, K.M, Lundesgaard, Ø., Renner, A.H.H, & Ingvaldsen, R.B. Suggested water mass defintions for the central and northern Barents Sea, and the adjacent Nansen Basin: Workshop Report. The Nansen Legacy Report Series 8 (2020).

[dataset] Søreide, J. CTD Data from Nansen Legacy Cruise—Seasonal Cruise Q4 (Norwegian Marine Data Centre, 2022); https://doi.org/10.21335/NMDC-301551919

Tesán Onrubia, J. A., Petrova, M. V., Puigcorbé, V., Black, E. E., Valk, O., Dufour, A., Hamelin, B., Buesseler, K. O., Masqué, P., Le Moigne, F. A. C., Sonke, J. E., van der Loeff, M. R., & Heimbürger-Boavida, L-E. Mercury export flux in the Arctic Ocean estimated from ^{234}Th: ^{238}U disequilibria. *ACS Earth and Space Chemistry* **4**, 795-801, https://doi.org/10.1021/acsearthspacechem.0c00055 (2020).

Thiele, S., Vader, A., Thomson, S., Saubrekka, K., Petelenz, E., Müller, O., Bratbak, G., & Øvreås, L. Seasonality of the bacterial and archaeal community composition of the Northern Barents Sea. *Frontiers in Microbiology* **14**, 1213718, https://doi.org/10.3389/fmicb.2023.1213718 (2023).

[dataset] Vader, A. Chlorophyll A and phaeopigments Nansen Legacy (Norwegian Marine Data Centre, 2022) https://doi.org/10.21335/NMDC-1371694848

Varty, S., Lehnherr, I., St Pierre, K., Kirk, J. & Wisniewski, V. Methylmercury transport and fate shows strong seasonal and spatial variability along a high Arctic freshwater hydrologic continuum. *Environmental Science & Technology* **55**, 331-340, https://doi.org/10.1021/acs.est.0c05051 (2021).

Villar, E., Cabrol, L. & Heimburger-Boavida, L-E. Widespread microbial mercury methylation genes in the global ocean. *Environmental Microbiology Reports* **12**, 277-287, https://doi.org/10.1111/1758-2229.12829 (2020).

Vlassopoulos, D., Kanematsu, M., Henry, E. A., Goin, J., Leven, A., Glaser, D., Brown, S. S., & O'Day, P. A. Manganese(iv) oxide amendments reduce methylmercury concentrations in sediment porewater. *Environmental Science: Processes & Impacts* **20**, 1746-1760, https://doi.org/10.1039/c7em00583k (2018).

Wang, F., Macdonald, R. W., Armstrong, D. A. & Stern, G. A. Total and methylated mercury in the Beaufort Sea: the role of local and recent organic remineralization. *Environmental Science & Technology* **46**, 11821-11828, https://doi.org/10.1021/es302882d (2012).

Wang, K., Munson, K. M., Beaupré-Laperrière, A., Mucci, A., Macdonald, R. W., & Wang, F. Subsurface seawater methylmercury maximum explains biotic mercury concentrations in the Canadian Arctic. *Scientific Reports* **8**, 1-5, https://doi.org/10.1038/s41598-018-32760-0 (2018).

Xiang, Y. & Lam, P. J. Size-fractionated compositions of marine suspended particles in the Western Arctic Ocean: Lateral and Vertical Sources. *Journal of Geophysical Research: Oceans* **125**, e2020JC016144, https://doi.org/10.1029/2020JC016144 (2020).

Yue, F., Angot, H., Blomquist, B., Schmale, J., Hoppe, C. J. M., Lei, R., Shupe, M. D., Zhan, L., Ren, J., Liu, H., Beck, I., Howard, D., Jokinen, T., Laurila, T., Quélever, L., Boyer, M., Petäjä, T., Archer, S., Bariteau, L., Helmig, D., Hueber, J., Jacobi, H-W., Posman, K., & Xie, Z. The Marginal Ice Zone as a dominant source region of atmospheric mercury during central Arctic summertime. *Nature Communications* **14**, 4887 https://doi.org/10.1038/s41467-023-40660-9 (2023).

Zhang, Y. X., Soerensen, A. L., Schartup, A. T. & Sunderland, E. M. A global model for methylmercury formation and uptake at the base of marine food webs. *Global Biogeochemical Cycles* **34**, e2019GB006348, https://doi.org/10.1029/2019GB006348 (2020)

Zolkos, S., Krabbenhoft, D. P., Suslova, A., Tank, S. E., McClelland, J. W., Spencer, R. G. M., Shiklomanov, A., Zhulidov, A. V., Gurtovaya, T., Zimov, N., Zimov, S., Mutter, E. A., Kutny, L., Amos, E., & Holmes, R. M. Mercury export from Arctic great rivers. *Environmental Science & Technology* **54**, 4140-4148, https://doi.org/10.1021/acs.est.9b07145 (2020).

Supplementary Material

Biotic transformation of methylmercury at the onset of the Arctic spring bloom

Stephen G. Kohler[a], Lars-Eric Heimbürger-Boavida[b], Philipp Assmy[c], Oliver Müller[d], Stefan Thiele[d,e], Maria G. Digernes[a], Kuria Ndungu[f], Murat V. Ardelan[a]

[a]Department of Chemistry, Norwegian University of Science and Technology (NTNU), Høgskoleringen 5, NO-7491 Trondheim, Norway
[b]Aix-Marseille Université, CNRS/INSU, University de Toulon, IRD, Mediterranean Institute of Oceanography (MIO), Bât. Méditerranée, Campus de Luminy-Océanomed, 13009 Marseille, France
[c]Norwegian Polar Institute, Fram Centre, 9296, Tromsø, Norway
[d]Department of Biological Sciences, University of Bergen, Thormøhlensgate 53 A/B, 5006 Bergen, Norway
[e]Bjerknes Centre for Climate Research, Jahnebakken 5, 5007 Bergen, Norway
[f]Norwegian Institute for Water Research (NIVA), Økernveien 94, NO-0579 Oslo, Norway

Integration of THg and MeHg

We used trapezoidal integration for the upper 100 m in the water column for both THg and MeHg concentrations (Kohler et al., 2022). We assumed that the first available sampling depth (10 m or UIW depending on station) represented the sea ice-ocean interface (0 m) or the atmosphere-ocean interface (0 m). For 100 - 200 m integration, stations P2 and P5 were integrated to bottom sampling depths less than 200 m. Stations were linearly interpolated to 100 m using the closest available sampling depths. The exact sampling dates and days between for each station were used to calculate the rate constants and ΔMeHg values. Where MeHg samples were less than the LOD or LOQ, the LOD (2 fmol L^{-1}) and LOQ (7 fmol L^{-1}) were used as the sample depth's concentration for integration, respectively. As most samples are run in singles, uncertainty in Δ (±1SD) for late winter and spring ΔMeHg and ΔTHg was calculated using the absolute THg reproducibility reported (± 0.05 pmol L^{-1}) and absolute MeHg reproducibility reported (± 7 fmol L^{-1}) for all depths and propagated using the sum of squares method for integration, and reported as ± 1 SD.

Depth matching for environmental parameters

THg and MeHg sampling geographic coordinates and depths differ slightly from environmental parameter sampling geographic coordinates due to ship drift during multiple samplings. Station samplings were assumed to be identical despite multiple sampling CTD casts and deviance from exact coordinates. For Spearman rank analysis, regression analysis, and PCA, environmental data were linearly interpolated to sampling depths of THg and MeHg for each cruise using the closest sampling depths when necessary. Otherwise, matching depths were assumed to be from the same water parcel for data analysis.

Percentage of ΔMeHg calculations

Photodemethylation

Delta photodemethylation (Table S6, $\Delta MeHg_{pd}$, pmol m^{-2} d^{-1}) was estimated using a similar equation (1) as Kim et al., 2020. MeHg concentrations (C_{MeHg}, pmol L^{-1}) at each station were linearly interpolated for each depth in the surface 100 m in late winter using our observed concentrations at discrete depths. The photodemethylation rate was estimated based on satellite PAR (I_0, 15 E m^{-2} d^{-1}) in the region in April 2021 multiplied by the photodemethylation rate constant (k_{pd}, 0.001 m^2 E^{-1}) (Lehnherr et al., 2011). The k_{pd} was assumed constant over 100 m, while PAR (I) was attenuated by depth (z) using equation (2) found in Kim et al., 2020, with original reference Paulson and Simpson 1977, type I (clear water). We accounted for the sea ice coverage by multiplying by the average fraction of open water (f_{OW}) at each station in the previous 60 days from sampling in May, assuming zero transmittance through snow-covered sea ice.

$$\Delta MeHg_{pd} = \int_0^{100} \quad C_{MeHg} * (f_{OW} * PAR * k_{pd}) \tag{1}$$

$$\frac{I}{I_0} = Re^{\frac{z}{\xi_1}} + (1-R)e^{\frac{z}{\xi_2}} \tag{2}$$

Scavenging of MMHg

Delta MMHg scavenging (Table S5, $\Delta MeHg_{scav}$, pmol m^{-2} d^{-1}) was estimated using several assumptions. First we calculated pHg in the upper 100 m using our THg concentrations at each discrete depth in late winter. To do this, we used in situ POC concentrations (Marquardt 2022a, 2022b) at each sampling depth as a proxy for total particulate matter and K_d for Hg in the Arctic shelf ($1.38*10^6$ L kg^{-1}, Tesán Onrubia et al., 2020) to calculate dHg (3) and pHg (4). We also assumed that K_d does not change seasonally nor with depth. Then, we assumed that pMMHg makes up approximately 4% of pHg (Agather et al., 2019). We used our estimated pMMHg and POC concentrations to estimate a pMMHg/TPM ratio in the upper 100 m, by assuming that POC in late winter makes up approximately 25% of TPM (Dybwad et al., 2022). We used the average late winter POC fluxes reported in Bodur et al., 2023 using a short term sediment trap method (27 mg C m^{-2} d^{-1}) and assumed it represented 25% TPM flux of 108 mg m^{-2} d^{-1}, which is in agreement with previous TPM fluxes in the area determined by long term moorings (Dybwad et al., 2022). As POC fluxes were not attenuated with depth in late winter (Bodur et al., 2023), we multiplied our average pMMHg/TPM ratio by our estimated TPM flux to calculate a pMMHg flux at 100 m depth (5), for an average of 0.76 ± 0.06 pmol m^{-2} d^{-1} for $\Delta MeHg_{scav}$.

$$dHg = \frac{THg}{((K_d * POC) + 1)} \tag{3}$$

$$pHg = THg - dHg \tag{4}$$

$$\Delta\ MeHg_{scav} = pMMHg_{TPM} * TPM\ flux \tag{5}$$

Evasion of DMHg

We followed a similar approach to Kim et al., 2020 (and references therein) for calculating delta DMHg evasion (Table S6, $\Delta MeHg_{ev}$) (6). This included using estimated windspeeds from Longyearbyen airport in March and April 2021 (~ 8 m s^{-1}), surface water temperatures (~ 10 m depth), at each station in late winter, temperature dependent Schmidt numbers for CO_2 and DMHg to calculate the DMHg transfer coefficient (K_w), and temperature dependent Henry's law constant for DMHg (H). We estimated the DMHg ($C_{DMHg\ water}$) concentration in surface waters using the % DMHg as MeHg as reported by Jonsson et al., 2022 (~ 6% in primary mixed layer) at shallowest sample depth for MeHg in late winter, and a literature value of 0.023 pmol m^{-3} for DMHg in air ($C_{DMHg\ air}$, Baya et al., 2015). We multiplied our estimated DMHg evasion flux by the average fraction of open water (f_{OW}) in the previous 60 days at each station from sampling in May, assuming sea ice completely restricts atmospheric evasion (DiMento et al., 2019).

$$\Delta MeHg_{ev} = K_w * [C_{DMHg_{water}} - \left(\frac{C_{DMHg_{air}}}{H}\right)] * f_{OW} \tag{6}$$

Dark demethylation

We calculated percentage dark methylation ($\Delta MeHg_{dark}$) as the proportion of ΔMeHg unaccounted for from the sum of $\Delta MeHg_{pd}$, $\Delta MeHg_{scav}$ and $\Delta MeHg_{ev}$ for each station.

Flow cytometry (FCM) Analysis

To measure the abundance of microorganisms (prokaryotes [bacteria and archaea], pico- and nanophytoplankton), four replicate water samples (1.8 mL) were taken, fixed with glutaraldehyde (0.5 % final concentration) at 4 °C for a minimum of 2 h, flash-frozen in liquid nitrogen and stored at -80 °C until analysis. Samples for the analysis of prokaryote abundance were first diluted 10 times with 0.2-µm-filtered TE buffer (Tris 10 mM and EDTA 1 mM, pH 8), then stained with a green fluorescent nucleic acid dye (SYBR Green I; Molecular Probes, Eugene, OR, USA) and incubated for 10 min at 80 °C and measured on a FACS Calibur (Becton Dickinson, Oxford, UK) flow cytometer (Marie et al., 1999). Samples were counted at a low flow rate of around 60 µL min-1 and groups discriminated on a biparametric plot of green fluorescence (BL1) vs. side scatter (SSC). Pico- and nanosized phytoplankton abundance was measured using an Attune® Acoustic Focusing Flow cytometer (Applied Biosystems by Thermo Fisher Scientific, Waltham, MA, USA) and the different phytoplankton groups were discriminated based on their red fluorescence (BL3) vs. orange fluorescence (BL2) (Paulsen et al., 2016). The data for all cruises can be found at the Norwegian Marine Data Centre (Mùller et al., 2023a, 2023b, 2023c, 2023d).

Bacterial Community Analysis

We investigated the bacterial and archaeal community with respect to potential demethylators (Christakis et al., 2018), methanotrophs, and sulfate reducing bacteria (SRB) using 16S rRNA gene amplicon sequences collected on our transect to help explain the MeHg concentrations at different depths. Using PICRUSt2 with standard parameters in bioconda, the metabolic potential of the different amplicon sequence variants was inferred based on their location in a phylogenetic tree of fully sequenced organisms and the genomic assets of the closest relative in this tree (Grüning et al., 2018, Douglas et al., 2020). Using KEGG-numbers, the marker genes *merA* and *merB* (reductive demethylation), *dsrA* (sulfate reduction), and *mmoX* (methanotrophy) were extracted and used to identify SRB, methanogens, and methanotrophs. For *merA* and *merB,* only *Oleibacter* was identified from the samples and was complemented with manual searches for *Alteromonas* and *Marinobacter* (Sanz-Sáez et al., 2022). Similarly, no *mmoX* genes were predicted and known methanotrophs were extracted based on recent literature (Guerrero-Cruz et al., 2021). SRB were well covered by the PICRUSt2 results. In the water column, the relative abundance of potential reductive demethylators and SRB was highest in the deepest sample of station P7 with 1.9% and 0.7% (potential reductive demethylators) and 4.8% and 3.9% (SRB) in late winter and spring. Potential reductive demethylators were otherwise low in relative abundance, rarely exceeding 0.1% of the total bacterial and archaeal community. Higher abundance was found in most samples at 10 m and below 200 m depth as compared to the samples in between, regardless of bottom depth for both seasons, although on average the abundance was higher in late winter (~0.1%) than in spring (~0.06%). SRB were similarly abundant in both seasons with 0.39% in late winter and 0.37% in spring but were lower in surface samples (10 and 20 m) as compared to deeper samples. Methanotrophs were also low in abundance with ~0.15% both in late winter and spring. The highest abundance was found in both seasons at P1 (near bottom depth) with 1.3% in spring as compared to 0.7% in late winter. Generally, the abundance was higher in samples > 20 m.

Dissolved Organic Matter (DOM) Analysis

DOM seawater and under ice water samples were collected at stations P1, P4, P6, and P7 on both late winter and spring sampling expeditions. Water samples were immediately extracted after collection using solid phase extraction (Dittmar et al., 2008) and stored at -20°C until analysis. Extracts were analyzed by LTQ-Velos-Pro Orbitrap mass spectrometer (Thermo Scientific, Germany) with an electrospray ionization source (ESI) in negative mode. Each sample spectrum was calibrated internally in mass range 200-800 m/z with data resolution of 100 000. Additional detailed instrument parameters are noted in Hawkes et al., 2016. Dissolved organic sulfur compounds (CHOS) formulas are determined based on the following elemental criteria: $C_{4\text{-}50}H_{4\text{-}100}O_{2\text{-}40}N_{0\text{-}2}S_{0\text{-}1}$, hydrogen to carbon ratio (H/C) = 0.3 - 2.2, oxygen to carbon ratio (O/C) = 0-1, double bond equivalent-oxygen (DBE-O) = -10 - 10, valence electron as even number, mass to charge ratio (m/z) = 150-800 and mass defect (mass after nominal mass) = -0.1 - 0.3.

References

[dataset] Assmy, P., Gradinger, R., Edvardsen, B., Wold, A., Goraguer, L., & Wiktor, J. Phytoplankton biodiversity Nansen Legacy Q1 (Norwegian Polar Institute, 2022a) https://doi.org/10.21334/npolar.2022.e6521515

[dataset] Assmy, P., Gradinger, R., Edvardsen, B., Wold, A., Goraguer, L., Wiktor, J., Tatarek, A., & Smoła, Z. Phytoplankton biodiversity Nansen Legacy Q2 (Norwegian Polar Institute, 2022b) https://doi.org/10.21334/npolar.2022.9c05c643

Baya, P. A., Gosselin, M., Lehnherr, I., St Louis, V. L. & Hintelmann, H. Determination of monomethylmercury and dimethylmercury in the Arctic marine boundary layer. *Environmental Science & Technology* **49**, 223-232, https://doi.org/10.1021/es502601z (2015).

Bodur, Y. V., Renaud, P. E., Goraguer, L., Amargant-Arumí, M., Assmy, P., Dąbrowska, A., Marquardt, M., Renner, A. H. H., Tatarek, A., & Reigstad, M. Seasonal patterns of vertical flux in the northwestern Barents Sea under Atlantic Water influence and sea-ice decline. *Progress in Oceanography*, **219**, 103132, https://doi.org/10.1016/j.pocean.2023.103132 (2023).

Christakis, C. A., Barkay T., & Boyd E. S. Expanded diversity and phylogeny of mer genes broadens mercury resistance paradigms and reveals an origin for merA among thermophilic archaea. *Frontiers in Microbiology* **12**, 682605, https://doi.org/10.3389/fmicb.2021.682605 (2021).

DiMento, B. P., Mason, R. P., Brooks, S. & Moore, C. The impact of sea ice on the air-sea exchange of mercury in the Arctic Ocean. *Deep Sea Research Part I* **144**, 28-38, https://doi.org/10.1016/j.dsr.2018.12.001 (2019).

Dittmar, T., Koch, B., Hertkorn, N., & Kattner, G. A simple and efficient method for the solid-phase extraction of dissolved organic matter (SPE-DOM) from seawater. *Limnology and Oceanography: Methods* **6**, 230-235. https://doi.org/10.4319/lom.2008.6.230 (2008).

Douglas, G. M., Maffei, V. J., Zaneweld, J. R., Yurgel, S. N., Brown, J. R., Taylor, C. M., Huttenhower, C., & Langille, M. G. I. PICRUSt2 for prediction of metagenome functions. *Nature Biotechnology* **38**, 685-688, https://doi.org/10.1038/s41587-020-0548-6 (2020).

Dybwad, C., Lalande, C., Bodur, Y. V., Henley, S. F., Cottier, F., Ershova, E. A., Hobbs, L., Last, K. S., Dąbrowska, A. M., & Reigstad, M. The influence of sea ice cover and Atlantic

Water advection on annual particle export north of Svalbard. *Journal of Geophysical Research: Oceans* **127**, e2022JC018897, https://doi.org/10.1029/2022jc018897 (2022).

Grüning, B., Dale, R., Sjödin, A., Chapman, B. A., Rowe, J., Tomkins-Tinch, C. H., Valieris, R., Köster, J., & The Bioconda Team. Bioconda: sustainable and comprehensive software distribution for the life sciences. *Nature Methods* **15,** 475-476 https://doi.org/10.1038/s41592-018-0046-7 (2018).

Guerrero-Cruz, S., Vaksmaa, A., Horn, M. A., Niemann, H., Pijuan, M., & Ho, A. Methanotrophs: discoveries, environmental relevance, and a perspective on current and future applications. *Frontiers in Microbiology **12***, 678057, https://doi.org/10.3389/fmicb.2021.678057 (2021)

Hawkes, J. A., Dittmar, T., Patriarca, C., Tranvik, L., & Bergquist, J. Evaluation of the Orbitrap mass spectrometer for the molecular fingerprinting analysis of natural dissolved organic matter. *Analytical Chemistry* **88**, 7698-7704, https://doi.org/10.1021/acs.analchem.6b01624 (2016).

Jonsson, S., Nerentorp Mastromonaco, M. G., Gårdfeldt, K. & Mason, R. P. Distribution of total mercury and methylated mercury species in Central Arctic Ocean water and ice. *Marine Chemistry* **242**, 104105, https://doi.org/10.1016/j.marchem.2022.104105 (2022).

Kim, J., Soerensen, A. L., Kim, M. S., Eom, S., Rhee, T. S., Jin, Y. K., & Han, S. Mass budget of methylmercury in the East Siberian Sea: The Importance of Sediment Sources. *Environmental Science & Technology* **54**, 9949-9957, https://doi.org/10.1021/acs.est.0c00154 (2020).

Kohler, S. G. Heimbürger-Boavida, L-E., Petrova, M. V., Digernes, M. G., Sanchez, N., Dufour, A., Simić, A., Ndungu, K., & Ardelan, M. V. Arctic Ocean's wintertime mercury concentrations limited by seasonal loss on the shelf. *Nature Geoscience* **15**, 621-626, https://doi.org/10.1038/s41561-022-00986-3 (2022a).

Lehnherr, I., St Louis, V. L., Hintelmann, H. & Kirk, J. L. Methylation of inorganic mercury in polar marine waters. *Nature Geoscience* **4**, 298-302, https://doi.org/10.1038/Ngeo1134 (2011).

Marie, D., Brussaard, C. P. D., Thyrhaug, R., Bratbak, G., & Vaulot, D. Enumeration of marine viruses in culture and natural samples by flow cytometry. *Applied and Environmental Microbiology* **65**, 45–52, https://doi.org/10.1128/AEM.65.1.45-52.1999 (1999).

[dataset] Marquardt, M., Bodur, Y. V., Dubourg, P., & Reigstad, M. Concentration of particulate organic carbon (POC) and particulate organic nitrogen (PON) from the sea water and sea ice in the northern Barents Sea as part of the Nansen Legacy project, Cruise 2021703 Q1. (Norstore, 2022a) https://doi.org/10.11.582/2022.00053

[dataset] Marquardt, M., Bodur, Y. V., Dubourg, P., & Reigstad, M. Concentration of particulate organic carbon (POC) and particulate organic nitrogen (PON) from the sea water and sea ice in the northern Barents Sea as part of the Nansen Legacy project, Cruise 2021704 Q2. (Norstore, 2022b) https://doi.org/10.11.582/2022.00054

[dataset] Müller, O., Petelenz, E., Tsagkaraki, T., Langvad, M., Grytaas, A., & Bratbak, G. Flow cytometry measurements (abundance of virus, bacteria and small protists (primarily <20µm)) during Nansen Legacy cruise 2021703 (from March 2nd to 24th in 2021) in the Northern Barents Sea (2023a) https://doi.org/10.21335/NMDC-282686035

[dataset] Müller, O., Petelenz, E., Tsagkaraki, T., Langvad, M., Thiele, S., Olsen, L., & Bratbak, G. Flow cytometry measurements (abundance of virus, bacteria and small protists (primarily <20µm)) during Nansen Legacy cruise 2021704 (from April 27th to May 20th in 2021) in the Northern Barents Sea (2023b) https://doi.org/10.21335/NMDC-277392634

[dataset] Müller, O., Petelenz, E., Tsagkaraki, T., Langvad, M., Olsen, L., & Bratbak, G. Flow cytometry measurements (abundance of virus, bacteria and small protists (primarily <20µm)) during Nansen Legacy cruise 2019706 (from August 5th to 27th in 2019) in the Northern Barents Sea (2023c) https://doi.org/10.21335/NMDC-39569968

[dataset] Müller, O., Petelenz, E., Tsagkaraki, T., Langvad, M., Stabell, H., & Bratbak, G. Flow cytometry measurements (abundance of virus, bacteria and small protists (primarily <20µm)) during Nansen Legacy cruise 2019711 (from November 28th to December 17th in 2019) in the Northern Barents Sea (2023d) https://doi.org/10.21335/NMDC-2099951995

Paulsen, M.L., Doré, H., Garczarek, L., Seuthe, L., Müller, O., Sandaa, R-A., Bratbak, G., & Larsen, A. Synechococcus in the Atlantic gateway to the Arctic Ocean. *Frontiers in Marine Science* **3**, 191. https://doi.org/10.3389/fmars.2016.00191 (2016).

Paulson, C. A. & Simpson, J. J. Irradiance measurements in the upper ocean. *Journal of Physical Oceanography* **7**, 952-956, https://doi.org/10.1175/1520-0485(1977)007<0952:IMITUO>2.0.CO;2 (1977).

Sanz-Sáez, I., Pereira-García, C., Bravo, A. G., Trujillo, L., Pla i Ferriol, M., Capilla, M., Sánchez, P., Martín-Doimeadios, R. C. R., Acinas, S. G., & Sánchez, O. Prevalence of heterotrophic methylmercury detoxifying bacteria across oceanic regions. *Environmental Science & Technology* **56**, 3452-3461, https://doi.org/10.1021/acs.est.1c05635 (2022).

Schlitzer, R., 2021. Ocean Data View, odv.awi.de.

Tesán Onrubia, J. A., Petrova, M. V., Puigcorbé, V., Black, E. E., Valk, O., Dufour, A., Hamelin, B., Buesseler, K. O., Masqué, P., Le Moigne, F. A. C., Sonke, J. E., van der Loeff, M. R., & Heimbürger-Boavida, L-E. Mercury export flux in the Arctic Ocean estimated from ^{234}Th:^{238}U disequilibria. *ACS Earth and Space Chemistry* **4**, 795-801, https://doi.org/10.1021/acsearthspacechem.0c00055 (2020).

[dataset] Vader, A. Chlorophyll A and phaeopigments Nansen Legacy (Norwegian Marine Data Centre, 2022) https://doi.org/10.21335/NMDC-1371694848

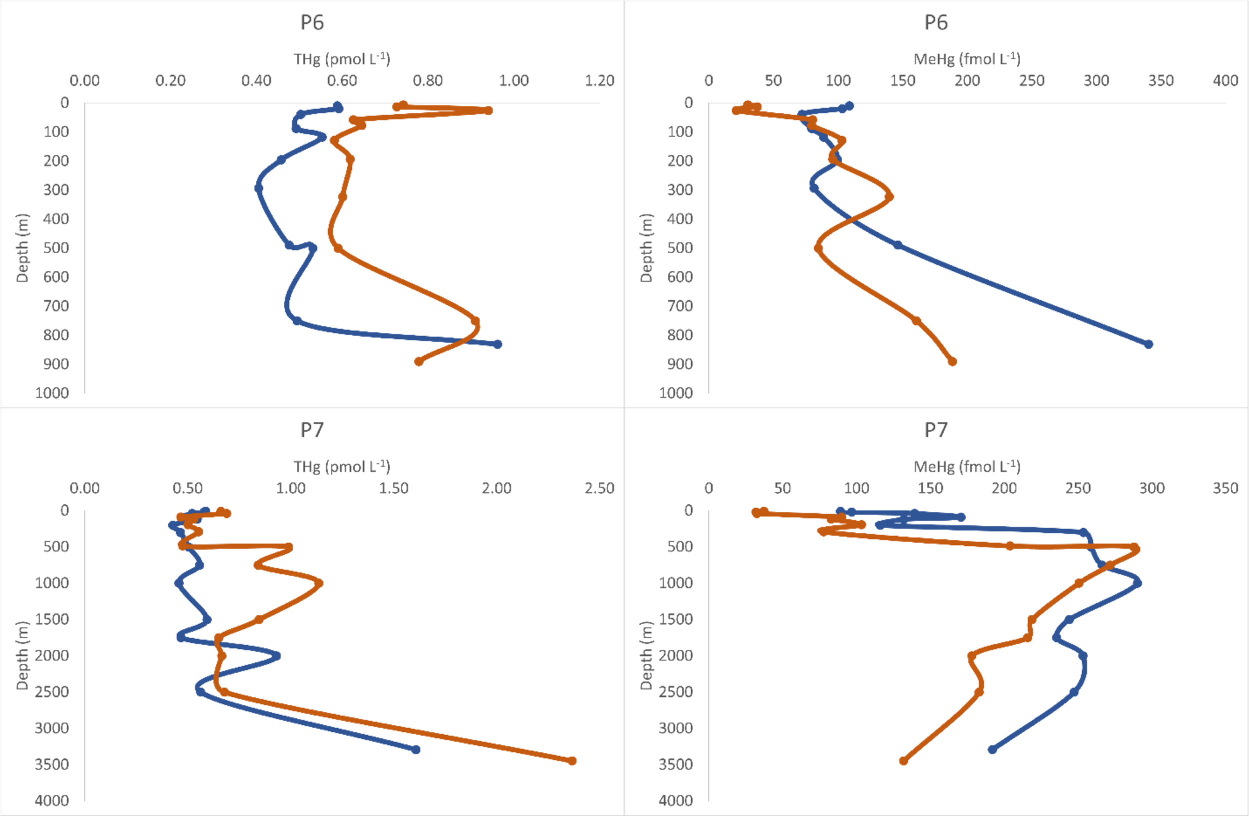

SI Figure 1: Complete depth profiles of THg (left, pmol L^{-1}) and MeHg (right, fmol L^{-1}) for stations P6 (top) and P7 (bottom) in late winter (blue) and spring (orange) in the northern Barents Sea in 2021.

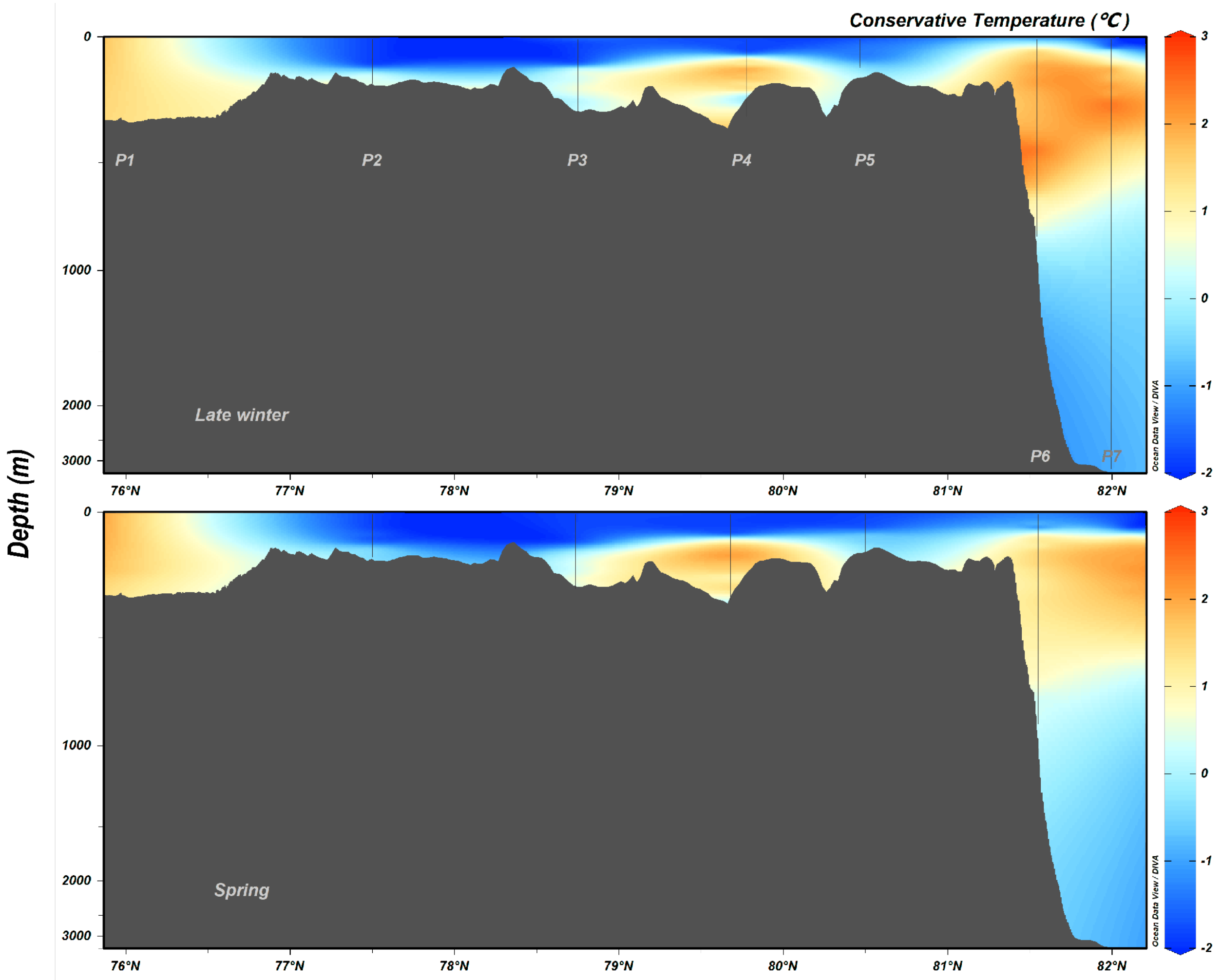

SI Figure 2: Conservative temperature (Θ, °C) along the shelf-basin transect in the northern Barents Sea during late winter (top) and spring (bottom) in 2021. The x-axis displays latitude and the nonlinear y-axis is in units of depth (m). Transect created with Ocean Data View (Schlitzer 2021).

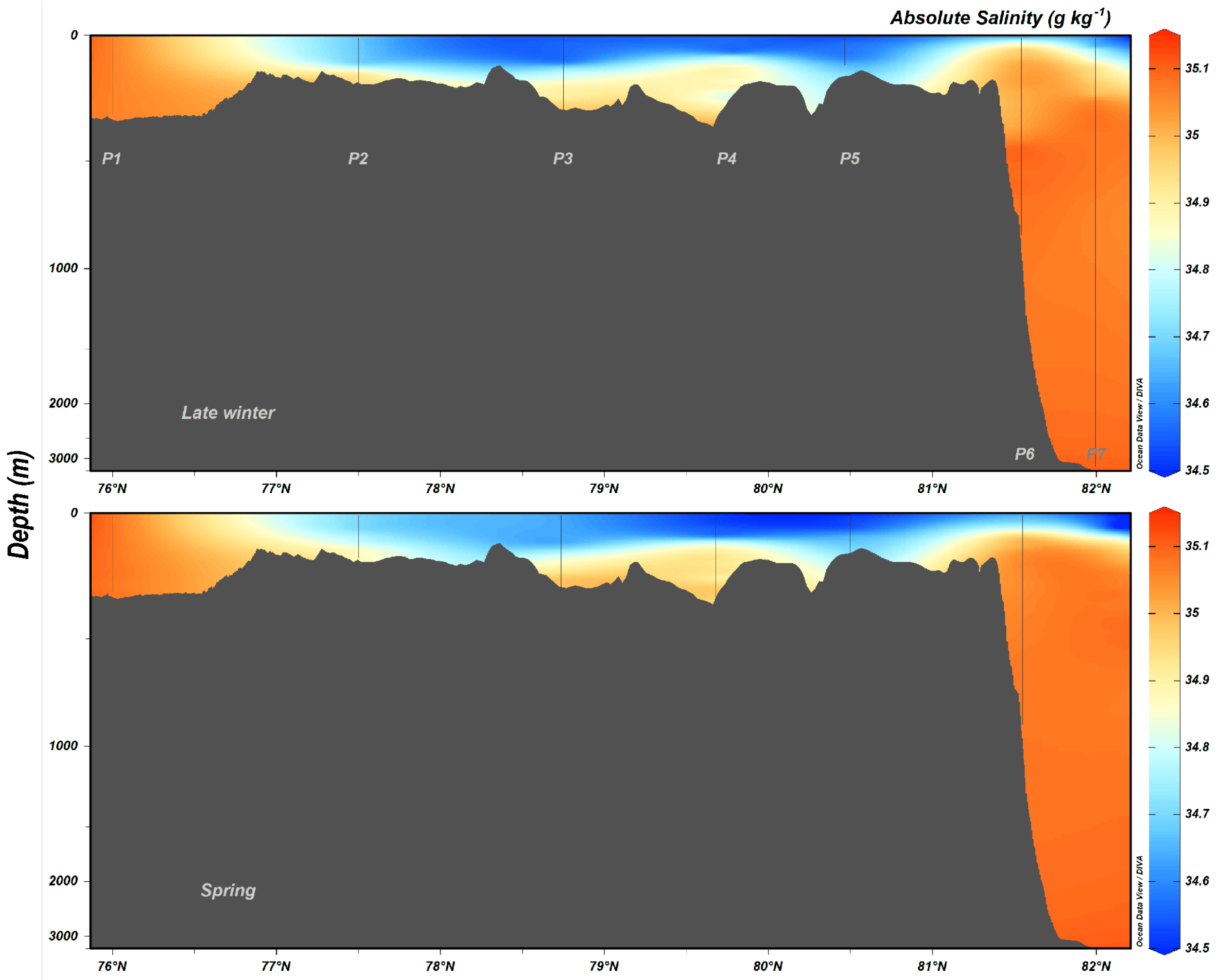

SI Figure 3: Absolute salinity (S_A, g kg^{-1}) along the shelf-basin transect in the northern Barents Sea during late winter (top) and spring (bottom) in 2021. The x-axis displays latitude and the nonlinear y-axis is in units of depth (m). Transect created with Ocean Data View (Schlitzer 2021).

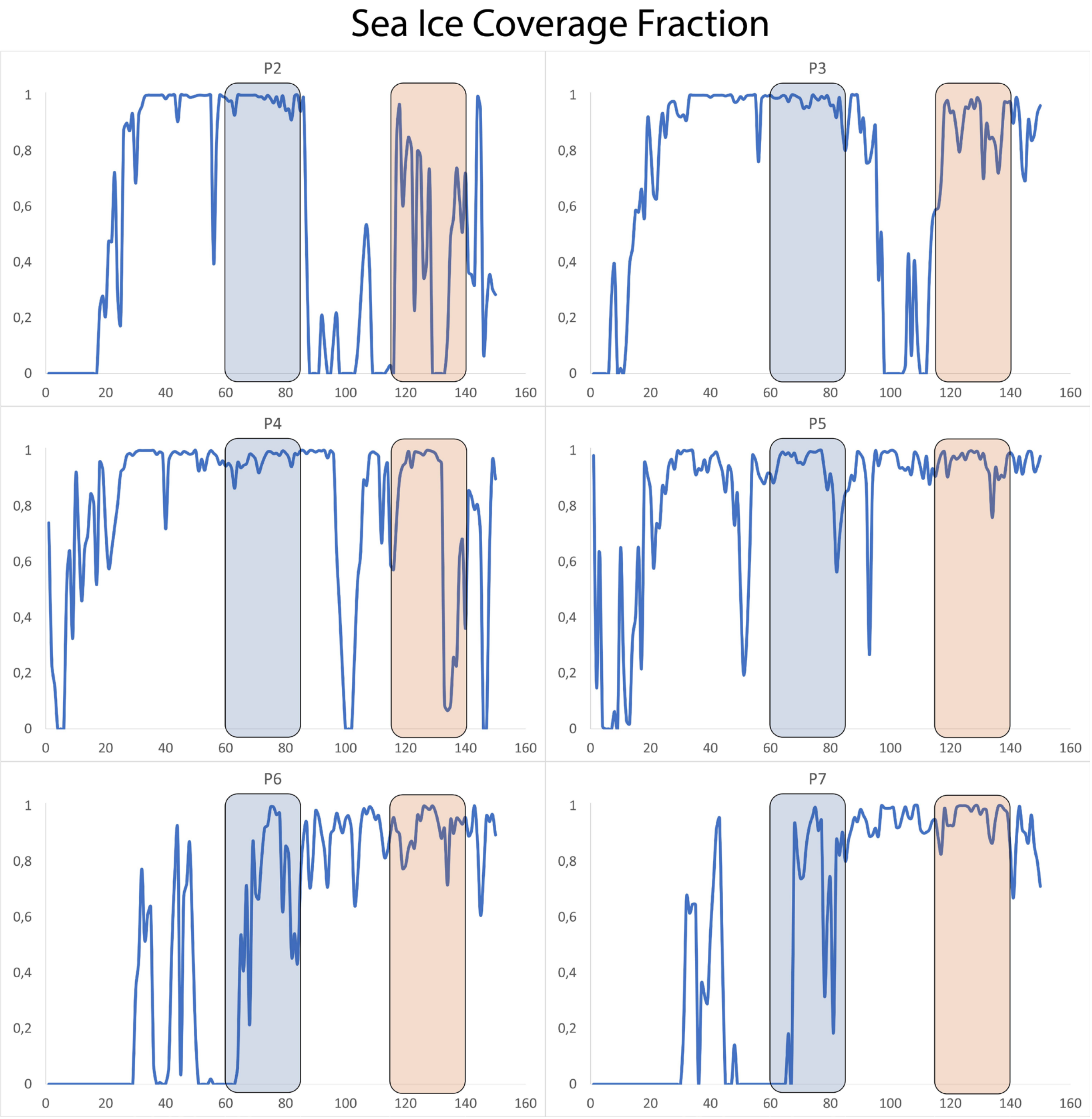

SI Figure 4: Fraction of sea ice coverage in the northern Barents Sea for stations P2 - P7 during January 1 - May 30, 2021. P1 had no ice coverage. An ice fraction of 1 indicates complete sea ice coverage and 0 indicates open water. Sampling periods are outlined in rectangles, with late winter (blue) and spring (orange). The y-axis is fraction of sea ice coverage (0 - 1) and the x-axis is in days starting from January 1, 2021.

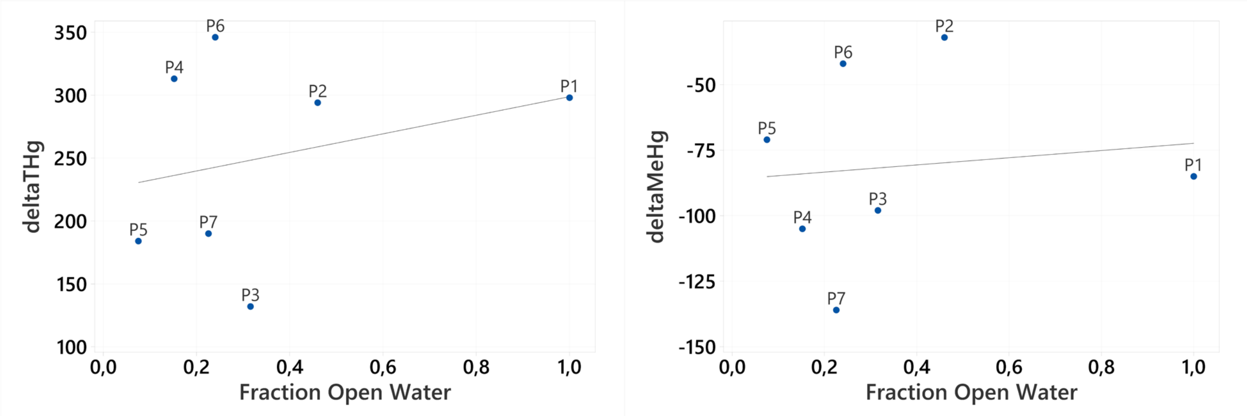

SI Figure 5: Linear regression of ΔTHg (pmol m^{-2} d^{-1}, left) and ΔMeHg (pmol m^{-2} d^{-1}, right) in the upper 100 m against the average fraction of open water in between sampling periods (60 day-average) in the northern Barents Sea in 2021. No significance (F-test, $p > 0.05$) was observed for either regression.

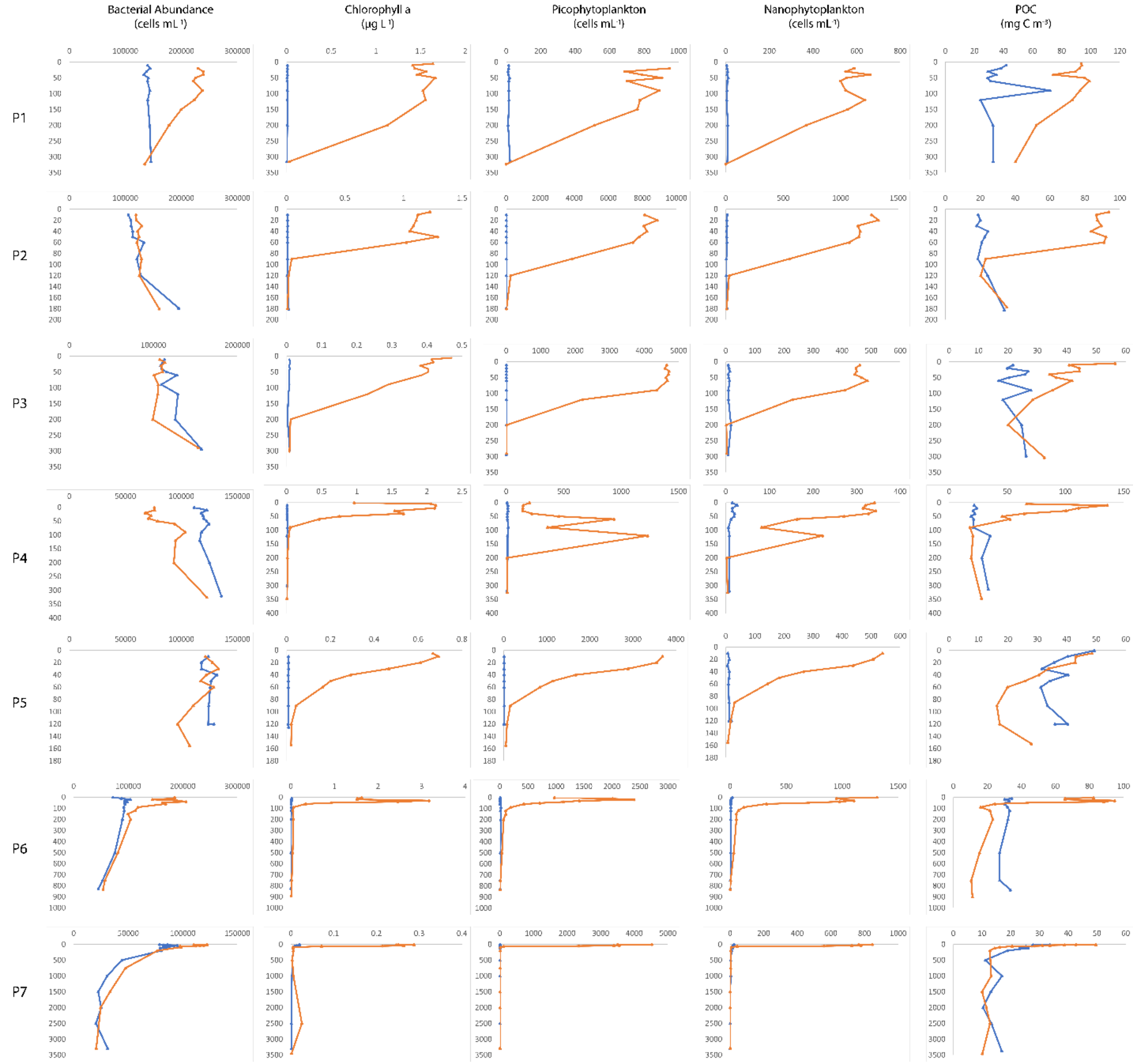

SI Figure 6: Bacterial abundance (cells mL^{-1}), chlorophyll *a* (µg L^{-1}), picophytoplankton abundance (cells mL^{-1}), nanophytoplankton abundance (cells mL^{-1}), and POC (mg C m^{-3}) for all seven stations (horizontal rows). Sampling periods are blue (late winter) and orange (spring). Each y-axis is in units of depth (m). Note the different scales in both x and y axes. Data from Marquardt 2022a, 2022b, Müller 2023a, 2023b, and Vader 2022.

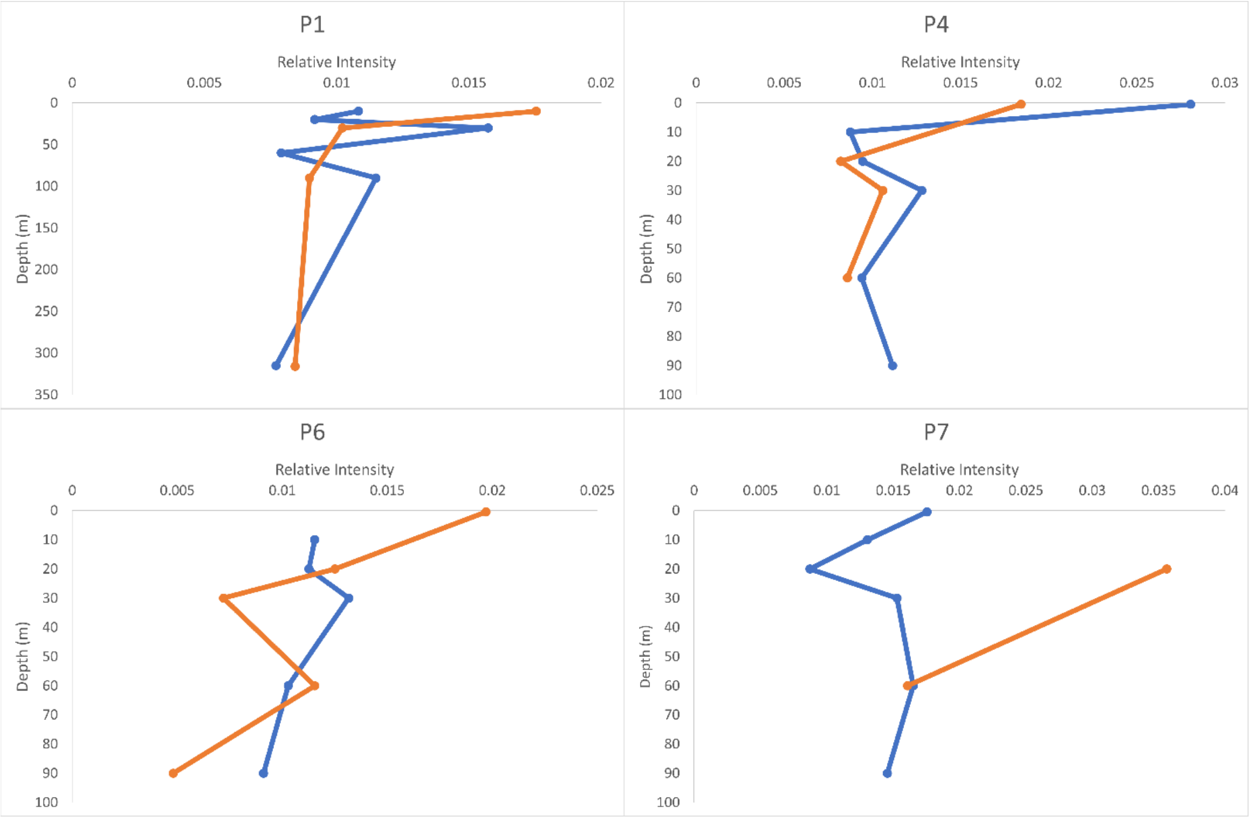

SI Figure 7: Relative intensities of dissolved organic sulfur compounds (CHOS) at selected stations on our transect in the northern Barents Sea for late winter (blue) and spring (orange). The y-axis is in units of depth and the x-axis is relative intensity. Note the different scales in both x and y axes.

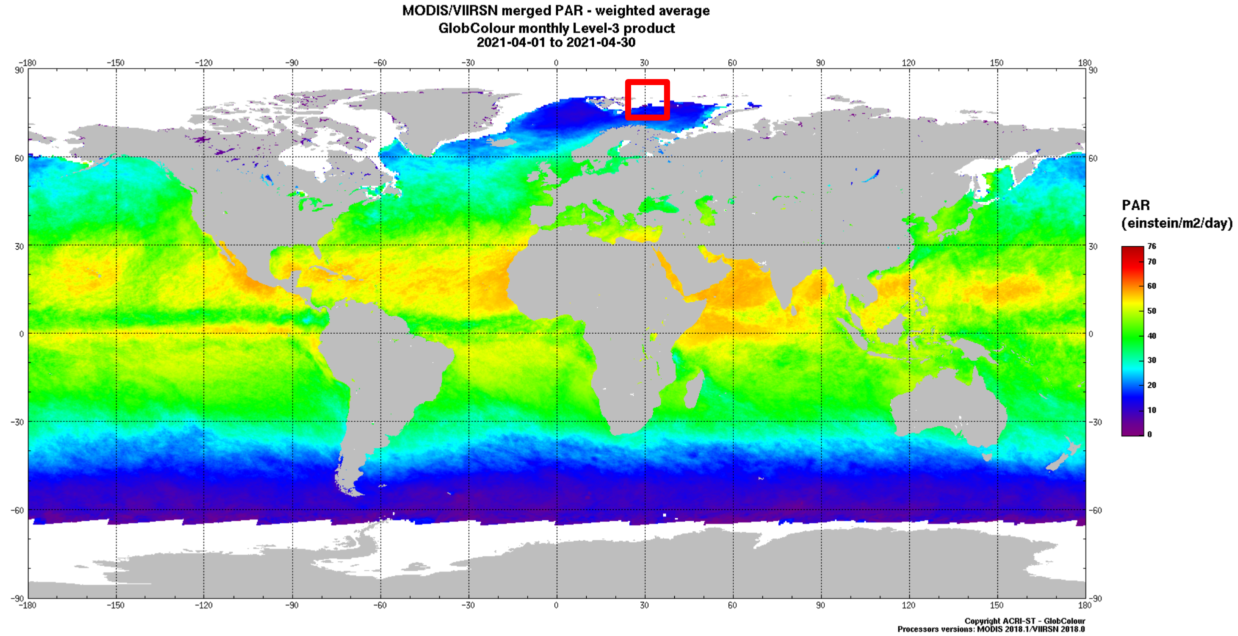

SI Figure 8: Satellite PAR (E m^{-2} d^{-1}) during the late winter and spring sampling periods (April 2021). PAR in the transect east of Svalbard (in red box), estimated to be approximately 15 E m^{-2} d^{-1} for all stations, despite significant ice coverage. Retrieved from GlobColour, Hermes, ocean surface optical PAR, © ACRI-ST – GlobColour (https://hermes.acri.fr/index.php?class=archive).

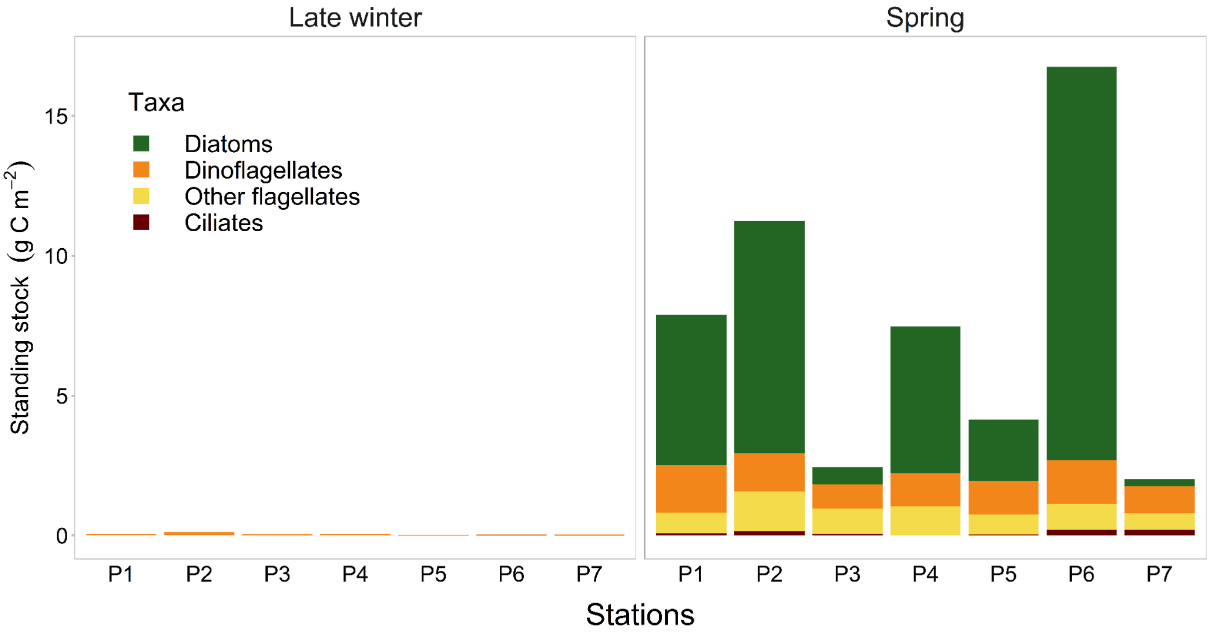

SI Figure 9: Integrated standing stocks (upper 90 m) of major protist groups (g C m^{-2}) during the late winter and spring sampling periods in the northern Barents Sea. The colors illustrate diatoms (dark green), dinoflagellates (orange), other flagellates (yellow) and ciliates (dark red). The x-axis shows each individual station. Data from Assmy 2022a, 2022b.

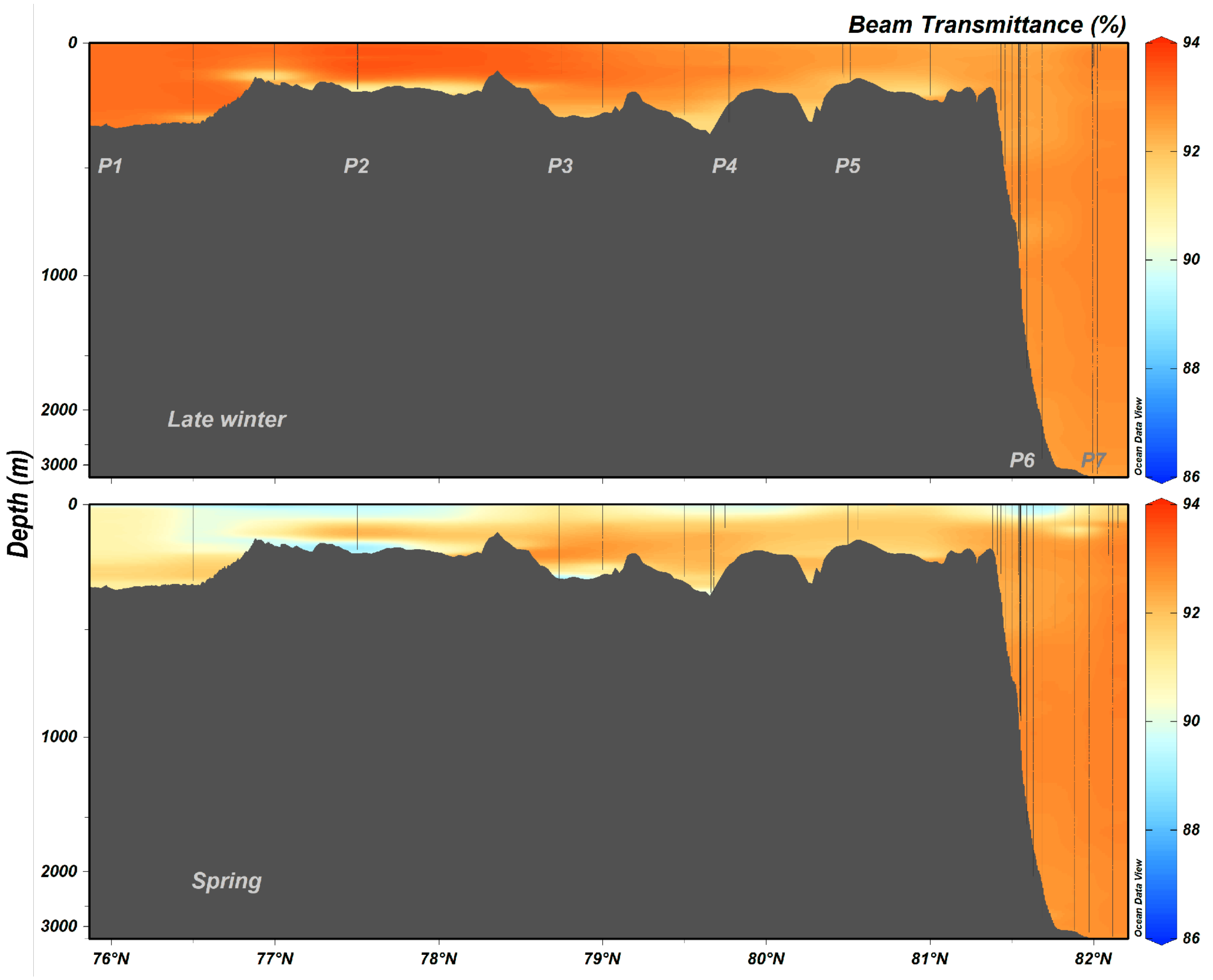

SI Figure 10: Raw beam transmittance (%), the fraction of light that reaches the detector, along the shelf-basin transect in the northern Barents Sea during late winter (top) and spring (bottom). A lower beam transmittance can indicate greater scattering or absorption by particles. The x-axis displays latitude and the nonlinear y-axis is in units of depth (m). Transect created with Ocean Data View (Schlitzer 2021).

Table S1: Average (± one standard deviation) of THg and MeHg concentrations on both late winter and spring cruises for water column samples above 500 m, categorized by water masses; Atlantic Water (AW), modified Atlantic Water (mAW), Polar Water (PW), warm Polar Water (wPW). Significant differences (log-transformed, Student's t-test, $p < 0.05$) between THg and MeHg in each respective season when categorized by water mass have each seasonal average marked with an asterisk (*).

	Total Hg (pmol L^{-1})		**Methylated Hg (fmol L^{-1})**	
Water mass	**Late winter**	**Spring**	**Late winter**	**Spring**
AW	0.47 ± 0.01 (n = 2)	N/A	200 ± 76 (n = 2)	N/A
mAW	0.53 ± 0.04* (n = 7)	0.64 ± 0.09* (n = 10)	63 ± 19 (n = 7)	57 ± 77 (n = 6)
PW	0.55 ± 0.07* (n = 26)	0.66 ± 0.08* (n = 34)	72 ± 30* (n = 26)	25 ± 14* (n = 31)
wPW	0.52 ± 0.07 (n = 14)	0.56 ± 0.07 (n = 12)	105 ± 37 (n = 14)	75 ± 36 (n = 12)

Table S2: Spearman rank correlation analysis (95% CI) for select environmental parameters for all stations and depths less than 500 m on the late winter cruise, with depth, total mercury (THg) methylated mercury (MeHg) particulate organic carbon (POC), chlorophyll *a* (Chla), nitrite (NO_2), nitrate (NO_3), phosphate (PO_4), silicate ($SiOH_4$), conservative temperature (Θ), absolute salinity (S_A), and bacteria. A significant p-value ($p < 0.05$) marked in bold.

	Depth	**THg**	**MeHg**	**POC**	**Chla**	**NO_2**	**NO_3**	**PO_4**	**$SiOH_4$**	**Θ**	**S_A**
THg	-0.097										
MeHg	**0.364**	0.03									
POC	0.037	0.201	0,095								
Chla	**-0.545**	**0.459**	-0.117	0,2							
NO_2	-0.077	**0.317**	**-0.315**	0.213	0.217						
NO_3	**0.623**	-0.053	**0.497**	**0.42**	**-0.323**	0.153					
PO_4	**0.545**	-0.025	**0.417**	**0.523**	-0.277	0.237	**0,957**				
$SiOH_4$	**0.588**	0.061	**0.565**	**0.455**	-0.204	0.135	**0,912**	**0.867**			
Θ	**0.63**	-0.243	**0.475**	**0.38**	**-0.429**	0	**0,889**	**0.833**	**0.817**		
S_A	**0.559**	-0.241	0.205	**0.294**	**-0.329**	0.082	**0,785**	**0.757**	**0.654**	**0.8**	
Bacteria	0.105	**0.298**	**-0.418**	0.267	0.133	**0.618**	0,113	0.249	0.037	-0.082	0.077

Table S3: Spearman rank correlation analysis (95% CI) for select environmental parameters for all stations and depths less than 500 m on the spring cruise, with depth, total mercury (THg) methylated mercury (MeHg) particulate organic carbon (POC), chlorophyll *a* (Chla), nitrite (NO_2), nitrate (NO_3), phosphate (PO_4), silicate ($SiOH_4$), conservative temperature (Θ), absolute salinity (S_A), and bacteria. A significant p-value ($p < 0.05$) marked in bold.

	Depth	**THg**	**MeHg**	**POC**	**Chla**	**NO_2**	**NO_3**	**PO_4**	**$SiOH_4$**	**Θ**	**S_A**
THg	**-0.609**										
MeHg	**0.394**	**-0.42**									
POC	**-0.622**	**0.714**	**-0.582**								
Chla	**-0.707**	**0.708**	**-0.467**	**0.895**							
NO_2	-0.05	0.045	**-0.308**	0.212	0.251						
NO_3	**0.66**	**-0.417**	**0.51**	**-0.489**	**-0.534**	-0.22					
PO_4	**0.724**	**-0.484**	**0.542**	**-0.59**	**-0.64**	-0.235	**0.937**				
$SiOH_4$	**0.668**	**-0.324**	**0.438**	**-0.389**	**-0.472**	-0.162	**0.938**	**0.897**			
Θ	**0.603**	**-0.414**	**0.378**	**-0.311**	**-0.315**	-0.081	**0.802**	**0.674**	**0.823**		
S_A	**0.649**	**-0.329**	**0.319**	-0.155	-0.255	-0.057	**0.723**	**0.621**	**0.724**	**0.856**	
Bacteria	-0.249	**0.469**	**-0.389**	**0.468**	**0.438**	-0.061	0.107	0.021	0.188	0.166	0.249

Table S4: Integrated THg pools (pmol m^{-2}) from 0 -100 m from all seasonal cruises completed in the area. We used data from Kohler et al. 2022a for summer and early winter.

	Integrated Total Hg pool (pmol m^{-2})			
0 - 100 m	**Late winter (March 2021)**	**Spring (May 2021)**	**Summer (August 2019)**	**Early winter (December 2019)**
P1	51647 ± 1696	68280 ± 1620	64033 ± 869	37050 ± 1736
P2	51197 ± 1620	67652 ± 1541	63050 ± 865	40050 ± 1800
P3	55570 ± 1620	63074 ± 1620	64483 ± 922	40267 ± 1829
P4	49786 ± 1601	67616 ± 1601	73635 ± 838	51400 ± 1866
P5	53409 ± 1677	63737 ± 1541	78773 ± 886	50136 ± 1753
P6	52700 ± 1994	72807 ± 1743	63300 ± 1115	43955 ± 2049
P7	52244 ± 2016	63251 ± 1989	55300 ± 1089	58200 ± 2200

Table S5: Integrated MeHg pools (pmol m^{-2}) from 0 -100 m from all seasonal cruises completed in the area. We used data from Kohler et al. 2022 for summer and early winter.

	Integrated Methylated Hg pool (pmol m^{-2})			
0 - 100 m	**Late winter (March 2021)**	**Spring (May 2021)**	**Summer (August 2019)**	**Early winter (December 2019)**
P1	5486 ± 237	710 ± 293	10133 ± 583	9350 ± 648
P2	3999 ± 227	2187 ± 216	10000 ± 604	9513 ± 731
P3	6912 ± 227	1341 ± 260	10317 ± 583	9450 ± 555
P4	7339 ± 224	1378 ± 245	9444 ± 548	9433 ± 583
P5	6611 ± 235	2640 ± 216	9550 ± 547	11000 ± 547
P6	8297 ± 279	5878 ± 244	13000 ± 679	10290 ± 624
P7	13381 ± 282	5485 ± 278	12850 ± 679	14350 ± 679

Table S6: ΔMeHg (pmol m^{-2} d^{-1}) for 0-100 m, calculated from 0 – 100 m integrated pools for late winter and spring. A negative value assigned in front of each ΔMeHg indicates in a negative change in the MeHg pool from late winter to spring, or a loss of MeHg.

Station	**Days between sampling**	**ΔMeHg pmol m^{-2} d^{-1}**	**ΔMeHg$_{pd}$ pmol m^{-2} d^{-1}**	**ΔMeHg$_{scav}$ pmol m^{-2} d^{-1}**	**ΔMeHg$_{ev}$ pmol m^{-2} d^{-1}**
P1	56	-85 ± 7	-10	-1	-7
P2	56	-32 ± 6	-3	-1	-2
P3	57	-98 ± 6	-3	-1	-2
P4	57	-105 ± 6	-1	-1	-1
P5	56	-71 ± 6	-1	-1	0
P6	58	-42 ± 6	-3	-1	-2
P7	58	-136 ± 7	-3	-1	-2

Table S7: Percent of variance explained for the first two plotted principal components for each cruise.

	% of Variance	
Cruise	**PC 1**	**PC 2**
Late Winter 2021 (LW)	43.3	20.2
Spring 2021 (SP)	52.8	17.0
Summer 2019 (SU)	56.5	12.1
Winter 2019 (W)	46.8	16.2